FARADAY PATTERNS IN SPIN-1 SPINOR BOSE-EINSTEIN CONDENSATES

Komal Sah

Advisor: Dr. Rejish Nath

Department of Physics
Indian Institute of Science Education and Research, Pune

A thesis submitted towards partial fulfillment of the
BS-MS Dual Degree Programme

April 2019

Certificate

This is to certify that this dissertation entitled **Faraday Patterns in Spin-1 Spinor Bose-Einstein Condensates** is submitted towards the partial fulfilment of the BS-MS dual degree programme at the Indian Institute of Science Education and Research, Pune represents study/work carried out by **Komal Sah** at Indian Institute of Science Education and Research under the supervision of **Dr. Rejish Nath**, Assistant Professor, Department of Physics, during the academic year 2018-2019.

Dr. Rejish Nath

Committee:
Dr. Rejish Nath
Dr. Umakant Rapol

This thesis is dedicated to Mum and Kemu

Declaration

I hereby declare that the matter embodied in the report entitled **Faraday Patterns in Spin-1 Spinor Bose-Einstein Condensates** are the results of the work carried out by me at the Department of Physics, **Indian Institute of Science Education and Research (IISER), Pune**, under the supervision of **Dr. Rejish Nath** and the same has not been submitted elsewhere for any other degree.

Komal Sah
April 2019

Acknowledgements

At the outset I would like to extend my gratitude to my thesis supervisor, Dr. Rejish Nath for his immense support, guidance and advice which helped steer the project in the right direction.

I would like to thank Dr. Umakant Rapol, for agreeing to supervise my project as the Thesis Advisor Committee member.

I am immensely grateful to Chinmayee for her patience in helping me with various aspects relating to the project throughout. Additionally, I would like to express my thanks to my lab members Ankita and Yashwant for the many insightful discussions.

I would also like to thank my friends and family for their constant support and encouragement.

I thank the Director, IISER Pune and the Dean (Graduate Studies), IISER Pune for all the facilities at the institute that enabled me to pursue the project in the first place.

Abstract

Vertical vibrations in classical liquids give rise to non-linear standing waves called Faraday waves when the driving frequency is greater than a critical value. An analogous phenomena is seen in Bose Einstein Condensates when the system's non-linearity is modulated and the uniform state loses it's stability to spatially modulated states. We study Faraday Patterns in Spin-1 Spinor Bose-Einstein Condensate on periodic modulation of the different s-wave scattering lengths, a_0 and a_2. The size of these patterns depends upon Bogoliubov mode resonant with half of the driving frequency. In case of Spin-1 Bose-Einstein Condensate the nature of Bogoliubov spectrum of spinor BECs depends explicitly on the magnetic ground state and also they are multi-branched with both spin and density modes, or coupling between them. The excitations of the spin-modes in some of the ground states leads to spin dynamics and formation of interesting spin-structures which have wavenumber indicative of the corresponding Bogoliubov mode. We find that by modulating the two scattering channels of spin-1 BEC with varied frequencies and amplitudes we can excite and explore different Bogoliubov modes of the spinor BEC.

Table of contents

List of figures

List of tables

Nomenclature

Acronyms / Abbreviations

AFM	Antiferromagnetic
BA	Broken Axisymmetry
BEC	Bose Einstein Condensates
FM	Ferromagnetic
GPE	Gross-Pitaevskii equation
P	Polar
Q2D	Quasi 2-Dimensional
sgn	Signum Function
SHO	Simple Harmonic Oscillator

Chapter 1

Introduction

1.1 Bose-Einstein Condensates

Bose-Einstein Condensates are formed when a large fraction of atoms in the system condense to the lowest energy state on the account of the system being cooled. This transition to a single quantum state can occur only if the atoms or particles posses a total integer spin such as $F = 0, 1, 2, ..$, referred to as "Bosons".

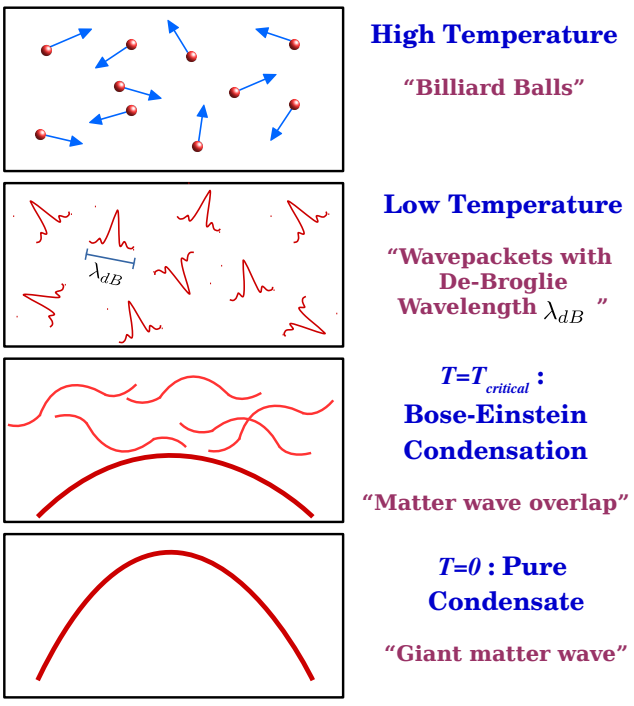

Fig. 1.1 Visualization of Bose-Einstein Condensation

This state of matter was first predicted in the 1920s by Albert Einstein and Satyendra Nath Bose. It was experimentally realized in dilute neutral atomic gases in 1995 by groups at JILA and the Massachusetts Institute of Technology (MIT) [1–3]. The spin in these first gaseous BECs was frozen in a single state as they were magnetically trapped. They were thus described by scalar order parameter $\psi(r,t)$.

1.2 Spinor Bose-Einstein Condensates

Optical trapping techniques were employed in 1997 to obtain condensates whose spins were not frozen in a single state called as spinor BEC [4]. The direction of atomic spins in an optical trap can change due to the interparticle interaction. As a result the order parameter of a spinor BEC is a vector that has $2f+1$ components $\Psi = (\psi_f, \psi_{f-1}, ...\psi_0, ..., \psi_{-f})$.

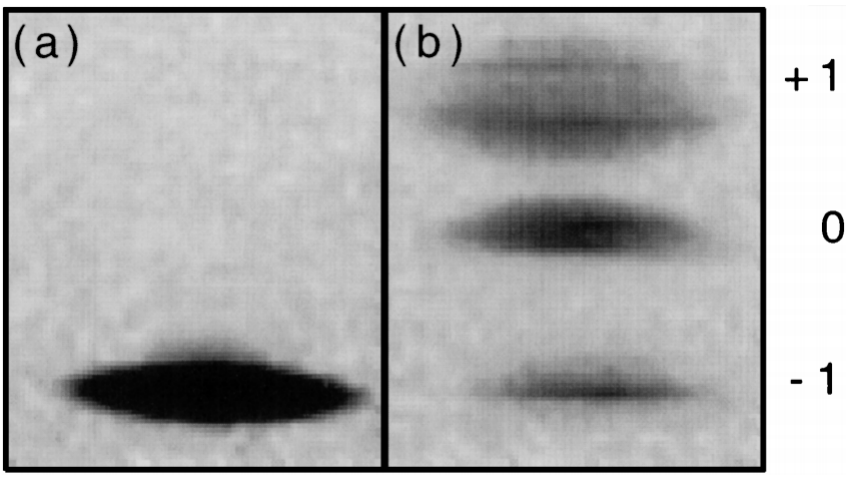

Fig. 1.2 (a)Spin-1 BEC in an optical trap,(b)Absorption image of the different components. (Taken from Figure 4. Phys. Rev. Lett. 80, 2027)

There are several consequences of this spin degree of freedom.The first being that below the critcal temperature required to create the BEC (T_{BEC}) there are several ground state phases possible and which one is realized depends upon the interaction parameters in the system. The number of ground state phases possible increases further in the presence of magnetic field [5–7]. The second consequence of this degree of freedom is that it allows for population exchange among the hyperfine states via the spin-exchange collisions. Lastly,the distribution of these spin vectors in space gives rise to different interesting structures or "spin-textures" such as vortex, skyrmion, spiral, helix etc [8–10].

Both degenerate and spinor Bose-Einstein condensates can be used as a powerful tool for simulating and studying physical effects with analogues throughout physics. Spinor BECs

which posses both magnetic ordering as well as superfluidity can be used to shed light on an array of topics such as the entanglement and squeezing of quantum fields, nonequilibrium quantum dynamics, quantum phase transitions and the role of symmetry and topology in quantum-ordered materials [11].

1.3 Project Development

1.3.1 Periodically driven BEC

Periodically driven classical systems such as the Kapitza pendulum and kicked rotor display rich dynamics and the study of their analogues in quantum systems [12] have had applications in photonic crystals [13], ion traps [14],irradiated graphene [15] and ultracold gases in optical lattices [16].

Periodic driving of s-wave scattering length in a BEC can be used to gain an insight into excitations of a BEC [17, 18]. Excitations in BEC are of two types - phonon like excitations (associated with long wavelengths) and particle like excitations (associated with higher wavelengths). The low lying excitations ,corresponding long wavelengths, that lead to collective excitation of the system are responsible for phenomenon of superfluidity and help understand the macroscopic behaviour of BECs. We study parametric resonance of the Bogoliubov mode in this excitation regime. The resonance is achieved by periodically modulating the non-linearity of the system. Translational symmetry breaking and pattern formation may be seen as a result of this modulation. The low lying excitations in spinor BEC show both phonon like and magnon like excitations which make it an interesting system to study using periodic driving.

Also, in the recent years there has been a resurrgence of research interests in periodically driven quantum systems such as BECs. Understanding periodic modulations in driven quantum systems is an essential component for Floquet engineering [12, 19, 20]. Parametric instabilities produced by periodic driving has been studied extensively in the context of a scalar condensate [21–23].

Periodic driving in spinor BEC has been studied by temporally modulating quadratic Zeeman coupling term [24]. In this project we explore a periodic driving in the s-wave scattering lengths of the system. The development and motivation behind the project is summarized in the next two sections.

1.3.2 Periodically driven Spin-1 Spinor BEC

Vertical vibrations in classical liquids give rise to non-linear standing waves called Faraday waves when the driving frequency is greater than a critical value. An analogous phenomena is seen in Bose Einstein Condensates when the system's non-linearity is modulated and the uniform state loses it's stability to spatially modulated states. Creating Faraday patterns in Bose Einstein condensates involves temporal periodic modulation of the s-wave scattering length. This leads to excitations of the sub-harmonic patterns in the atomic density through a parametric resonance resonance. The dominant wavelength of the instability and the symmetries of the selected patterns are intrinsic properties of the system, independent of (or only weakly dependent on the initial or boundary conditions). In case of BECs Faraday patterns offer important insights about the elementary excitations in BECs since the pattern size is determined by the Bogoliubov mode resonant with half of the driving frequency. Faraday pattern formation in spin-0 Bose Einstein Condensates has already been explored [18, 17]. The nature of Bogoliubov spectrum of spinor BECs depends explicitly on the magnetic ground state and also they are multi-branched with both spin and density modes, or coupled between them. We look at Faraday pattern formation in Spin-1 Bose Einstein Condensates which in addition to the density patterns also exhibits spin dynamics and shows interesting spin-textures when the spin modes are resonant with half the driving frequency. Also,in spinor BECs the two s-wave scattering channels with total spin-F $F = 0, 2$ may be modulated independently or together using the microwave-induced Feshbach resonance proposed in [25–30]. We look at Faraday pattern formation when each scattering channel is modulated independently, together with same amplitude and frequency and with different amplitude and frequency.

1.3.3 Overview

This section provides an overview of the work presented in this thesis. Chapter 1, introduces Spinor-BECs and periodic driving in quantum sytems. It discusses related works in this area. It briefly discusses how Faraday patterns may be used in studying elementary excitations in BECs and discusses motivation of the project.

Chapter 2, discusses the spin-1 BEC system i.e, the Hamiltonian of the system, the equation describing its dynamics (multicomponent GPE) and elementary excitations in the system. It then motivates how periodic driving can help study these excitations by studying Faraday Patterns. It also looks at Faraday Patterns in scalar BEC and scalar dipolar BEC.

The results and observations extend over Chapter 3,4,5. Since there are two scattering lengths involved here, a_0 and a_2 we consider three scenarios for time modulated scattering

lengths: (i) a_0 time-dependent and a_2 constant which is discussed in Chapter 3 (ii) a_0 constant and a_2 time-dependent which is discussed in Chapter 4 and finally (iii) both scattering lengths are time-dependent which id discussed in Chapter 5. Chapter 6 concludes the thesis and briefly discusses related work which can be pursued in the future.

Chapter 2

Theory

2.1 Hamiltonian of a Spin-1 BEC

The Hamiltonian describing a spin-1 BEC system can be divided into two parts:

- A non-interacting Hamiltonian which describes a single boson.
- An interaction Hamiltonian that describes the interaction between two bosons.

We discuss each of these parts separately before presenting the Hamiltonian describing the entire system. Ψ_m here represents the field operator of a spin-1 BEC where $m = 1, 0, -1$.

2.1.1 Non-Interacting Hamiltonian

$$\hat{H} = \int d^3r \sum_m \hat{\psi}_m^\dagger(r) \left(\frac{-\hbar^2}{2M} \bigtriangledown^2 + \hat{U}(r) \right) \hat{\psi}_m(r) + \hat{H}_z \tag{2.1}$$

The first term in the Hamiltonian represents the kinetic energy of the boson of mass 'M'.

$$\hat{U}(r) = \frac{M}{2}(\omega_z^2 z^2 + \omega^2(x^2 + y^2)) \tag{2.2}$$

The second term which is denoted by $\hat{U}(r)$ describes the trap potential. ω_z and ω represent the trap frequency in different directions. One can change the geometry of the trap by changing the taking values appropriate to realize the particular geometry. In our case we take a Quasi-2D trap which is attained by taking $\omega_z >> \omega$. The high value of trap in the z-direction confines the dynamics of the system to the other two directions effectively making the system 2-dimensional.

$$\hat{H}_z = \sum_{m,m'} \hat{\psi}_m^\dagger [-pF_z + qF_z^2]_{m,m'} \hat{\psi}_m \tag{2.3}$$

This last term gives the Zeeman splitting from an external magnetic field. The first term is the first order correction using perturbation theory while the second term is the second order perturbation. The value of p-coefficient of linear Zeeman effect is given as:

$$p = -\frac{\mu_B B}{2} \tag{2.4}$$

The quadratic zeeman term is composed of two parts. The first is q_B which is a contribution from the second order perturbation due to the applied magnetic field.

$$q_B = \frac{\mu_B^2 B^2}{\Delta E_{Hf}} \tag{2.5}$$

Here, ΔE_{Hf} is the hyperfine splitting energy. This contribution is positive. The second contribution is from a linearly polarised microwave field that induces a quadratic (ac) Zeeman shift of the order

$$q_u = \frac{-\hbar\Omega^2}{4\delta} \tag{2.6}$$

Here, Ω is the Rabi Frequency and δ is the detuning. The total quadratic Zeeman Energy is thus given as:

$$q = q_u + q_B \tag{2.7}$$

By changing the microwave field one can attain both negative and positive values of q. This has been experimentally explored in [31] [32] and [33]. This tuning of q allows us to look at not only different ground states of the spinor BEC but also study periodic driving [24] and quenching in spinor BEC systems [34].

2.1.2 Interaction Hamiltonian

Since BEC is realized in a very dilute gas we can ignore 3-body interactions. However, the two body interactions which define many properties of the BEC cannot be ignored. In a spin-1 BEC this two body interaction takes the form of spin-dependent scattering which conserves both total spin(F) and angular momentum(L). In a BEC interactions with $L > 0$ can be ignored. Hence we look at s-wave scattering alone. Collisions with spins can be written as :

$$\left\langle k, v_f \right| \hat{T} \left| k', v_{f'} \right\rangle \tag{2.8}$$

Here, f and f' are initial and final spin of the system with initial and final momentum k and k'.

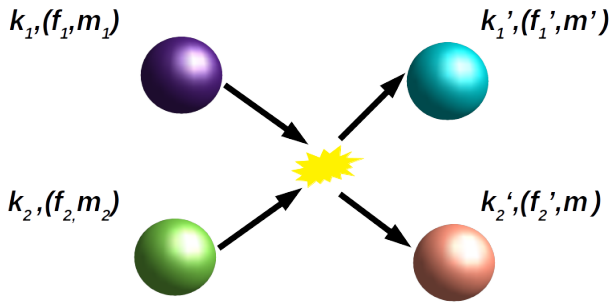

Fig. 2.1 Spin dependent scattering can change not only the momentum of the system but also the spin $|f,m>$ of the particles involved.

This interaction for a BEC can be written in terms of irreducible operators of the form,

$$V_F = \frac{1}{2}\int dr \int dr' \upsilon(r,r') \sum_{-F}^{F} \hat{A}^{\dagger}_{FM_s}(r,r') \hat{A}_{FM_s}(r,r') \tag{2.9}$$

Here, $\hat{A}_{F,M}(r,r')$ is an operator which destroys a pair of bosons at r and r' and is defined as:

$$\hat{A}_{FM_s}(r,r') = \sum_{m,m'=-f}^{f} \left\langle F,M_s|f,m;f,m'\right\rangle \hat{\psi}_m(r)\hat{\psi}_{m'}(r') \tag{2.10}$$

The position dependence of the interaction is given by the function below in which a_F is the scattering length of an interactions between bosons of total spin F.

$$\upsilon(r-r') = \frac{4\pi\hbar^2 a_F}{M}\delta(r-r') \tag{2.11}$$

The interaction equation can be simplified as:

$$V_F = \frac{1}{2}\int \sum_{m_1,m_2,m_1',m_2'} C^{m_1,m_2}_{m_1',m_2'} dr \hat{\psi}^{\dagger}_{m_1}(r)\hat{\psi}^{\dagger}_{m_2}(r)\hat{\psi}_{m_1'}(r)\hat{\psi}_{m_2'}(r) \tag{2.12}$$

Here the coefficient is defined as:

$$C_{m_1',m_2'}^{m_1,m_2} = \frac{4\pi\hbar^2}{M}\sum_{F=0,2} a_F \left\langle f,m_1;f,m_2\left|\hat{P}_F\right|f,m_1';f,m_2'\right\rangle \tag{2.13}$$

$$\hat{P}_F = \sum_{-F}^{F} |F,M_s><F,M_s| \tag{2.14}$$

The Projection operator can be written in the basis of spin density operator and density operator.

$$\hat{n} = (|\hat{\psi}_{-1}|^2+|\hat{\psi}_0|^2+|\hat{\psi}_1|^2) \tag{2.15}$$

$$\left|\hat{F}(r)\right|^2 = \hat{F}_x^2(r)+\hat{F}_y^2(r)+\hat{F}_z^2(r) \tag{2.16}$$

$$\hat{F}_{(\alpha=x,y,z)} = \sum_{m,m'} \hat{\psi}_m^\dagger (f_{(\nu=x,y,z)})_{m,m'}\hat{\psi}_{m'} \tag{2.17}$$

$$f_x = \frac{1}{\sqrt{2}}\begin{bmatrix}0&1&0\\1&0&1\\0&1&0\end{bmatrix} f_y = \frac{i}{\sqrt{2}}\begin{bmatrix}0&-1&0\\1&0&-1\\0&1&0\end{bmatrix} f_z = \begin{bmatrix}1&0&0\\0&0&0\\0&0&-1\end{bmatrix}$$

This give us the 2-body interaction Hamiltonian in a spin-1 BEC.

$$V_F = \frac{c_0}{2}\hat{n}^2(r)+\frac{c_1}{2}\left|\hat{F}(r)\right|^2 \tag{2.18}$$

c_0 and c_1 are magnitude of spin-independent and spin-dependent interaction. They are dependent on the scattering lengths a_0 (scattering length of channel with total spin $F=0$) and a_2 (scattering length of channel with total spin $F=2$) as:

$$c_0 = \frac{4\pi(a_0+2a_2)\hbar^2}{3M} \tag{2.19}$$

$$c_1 = \frac{4\pi(a_2-a_0)\hbar^2}{3M} \tag{2.20}$$

2.1.3 Spin-1 BEC total Hamiltonian

The complete Hamiltonian of the spin-1 BEC inclusive of both kinds of interactions is given as:

$$\hat{H} = \int d^3r \sum_m \hat{\psi}_m^\dagger(r)\left(\frac{-\hbar^2}{2M}\bigtriangledown^2+\hat{U}(r)\right)\hat{\psi}_m(r)+\hat{H}_z+\frac{c_0}{2}\hat{n}^2(r)+\frac{c_1}{2}\left|\hat{F}(r)\right|^2 \tag{2.21}$$

2.2 Mean Field theory - Spinor BECs

At very low temperatures, when the bosons condense to single state the field operator of the system can be written as:

$$\hat{\psi}_m = \psi_m + \delta\hat{\psi}_m \tag{2.22}$$

Here , ψ_m is the average number of particles in the lowest state $k = 0$. The number of particles in the other higher energy states represented by field operator $\delta\hat{\Psi}$ is negligible. Thus, the field operator can be replaced with the its expectation value which helps simplify the system.A large number of phenomena can be described with the mean field with reliable accuracy. A many-body approach though more accurate is difficult to work with. We use the mean field approximation to describe the system in our case.

2.3 Gross-Pitaevskii equations

The Gross-Pitaevskii equations is a Nonlinear Schrodinger Equation(NLSE) that describes the dynamics of the mean field. In the case of a spin-1 BEC, a coupled multi-component Gross-Pitaevskii equations(GPE) describes the system.

$$\begin{aligned} i\hbar\frac{d\psi_m}{dt} &= \frac{-\hbar^2\nabla^2\psi_m}{2M} + U(r)\psi_m + (-pm + qm^2)\psi_m \\ &\quad + c_0(|\psi_1|^2 + |\psi_0|^2 + |\psi_{-1}|^2)\psi_m + I_m \end{aligned} \tag{2.23}$$

$$I_+ = c_1(|\psi_0|^2 + |\psi_+|^2 - |\psi_-|^2)\psi_+ + c_1\psi_0^2\psi_-^* \tag{2.24}$$

$$I_0 = c_1(|\psi_+|^2 + |\psi_-|^2)\psi_0 + 2c_1\psi_+\psi_-\psi_0^* \tag{2.25}$$

$$I_- = c_1(|\psi_0|^2 - |\psi_+|^2 + |\psi_-|^2)\psi_- + c_1\psi_0^2\psi_+^* \tag{2.26}$$

We restrict ourselves to two dimensional space, which can be realized by considering a tight pancake shaped potential.In this case the axial confinement energy is so large that the dynamics in the z direction is frozen in the ground state of the strong harmonic potential. The procedure for reducing the dimensions is outlined in the Appendix. We get interaction parameters in 2-dimensions.

$$\tilde{c}_0 = c_0\sqrt{\frac{M\omega_z}{2\pi\hbar}} \tag{2.27}$$

$$\tilde{c}_1 = c_1\sqrt{\frac{M\omega_z}{2\pi\hbar}} \tag{2.28}$$

The 2-D GPE is given below:

$$\begin{aligned} i\hbar\frac{d\psi_m}{dt} &= \frac{-\hbar^2\nabla^2\psi_m}{2M}+\frac{M}{2}(\omega^2(x^2+y^2))\psi_m+(-pm+qm^2)\psi_m \\ &\quad +\tilde{c_0}(|\psi_1|^2+|\psi_0|^2+|\psi_{-1}|^2)\psi_m+I_m \end{aligned} \tag{2.29}$$

$$I_+ = \tilde{c}_1(|\psi_0|^2+|\psi_+|^2-|\psi_-|^2)\psi_+ +\tilde{c}_1\psi_0^2\psi_-^* \tag{2.30}$$

$$I_0 = \tilde{c}_1(|\psi_+|^2+|\psi_-|^2)\psi_0+2\tilde{c}_1\psi_+\psi_-\psi_0^* \tag{2.31}$$

$$I_- = \tilde{c}_1(|\psi_0|^2-|\psi_+|^2+|\psi_-|^2)\psi_- +\tilde{c}_1\psi_0^2\psi_+^* \tag{2.32}$$

The ground states of the spinor BEC in the mean field approximation is obtained by minimizing the multi-component GPE subject to the constraints of particle number conservation(N) and magnetization conservation F_z .The magnetization conservation arises as a consequence of conservation of total spin. We use the method of Lagrange multipliers to evaluate the ground states of the system analytically for different values of the parameters c_1, p and q. The Table-2.1 states the different ground state phases of spin-1 BEC and the phase diagram indicates structure of the ground-state spinor as a function of the linear p and quadratic q Zeeman energies.

2.3.1 Ground State Phases

- In the ferromagnetic phase all the population of the system is in the $m=1$ or $m=-1$ component.
- In the antiferromagnetic phase the population is divided between the $m=1$ or $m=-1$ components.
- In the polar phase all the population in the system is in the $m=0$ component.
- In the BA phase the population is divided unequally between the $m=1$, $m=-1$ and $m=0$ components.

2.4 Bogoliubov- de Gennes equations and elementary excitations

Weak excitations in the mean field ground state is described by Bogoliubov- de Gennes theory. To obtain the Bogoliubov excitation spectra we consider a small deviation to the

Ground States of Spin-1 BEC			
Phase	Order Parameter Ψ^T	f_z	$\tilde{\varepsilon} = \varepsilon - \frac{c_0 n}{2}$
(I) F	$(e^{i\chi_+}, 0, 0)$	1	$-p+q+\frac{c_1 n}{2}$
(II) F	$(0, 0, e^{i\chi_-})$	-1	$p+q+\frac{c_1 n}{2}$
(III) AF	$(e^{i\chi_+}\sqrt{\frac{1+\frac{p}{c_1}}{2}}, 0, e^{i\chi_-}\sqrt{\frac{1-\frac{p}{c_1}}{2}})$	$\frac{p}{c_1 n}$	$q-\frac{p^2}{2c_1 n}$
(IV) P	$(0, e^{i\chi_0}, 0)$	0	0
(V) BA	$(e^{i(\chi_0+\chi_z)}\frac{p\sqrt{f_z}(q+p)}{2}, e^{i\chi_0}\sqrt{\frac{(q^2-p^2)(-p^2-q^2+2c_1 nq)}{4c_1 nq^3}}, e^{i(\chi_0+\chi_z)}\frac{p\sqrt{f_z}(q-p)}{2})$	$\frac{p(-p^2+q^2+2qc_1 n)}{2c_1 nq^2}$	$\frac{(-p^2+q^2+2qc_1 n)^2}{8c_1 nq^2}$

Table 2.1 Ground state phases of Spin-1 BEC

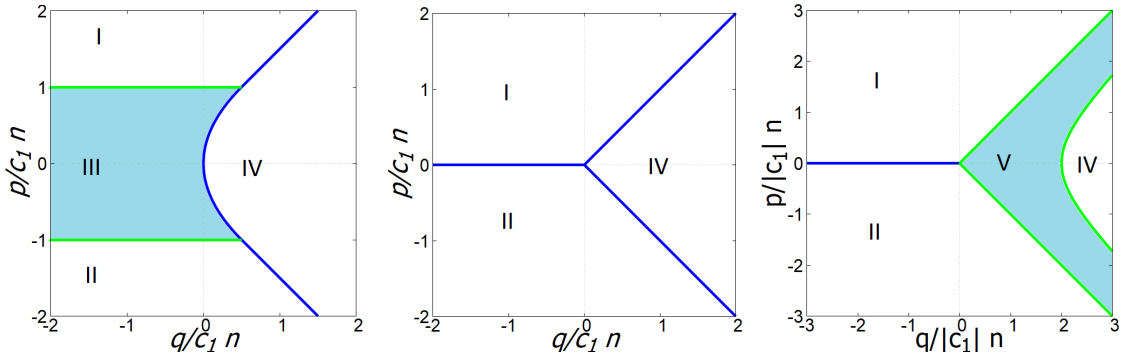

(a) $c_1 > 0$ (b) $c_1 = 0$ (c) $c_1 < 0$

Fig. 2.2 Phase diagram of ground states of the spin-1 BEC under (a)$c_1 > 0$ (b)$c_1 = 0$ (c)$c_1 < 0$

mean field value, obtained using the Gross-Pitaevskii equations .i.e,

$$\hat{\psi}_m = \psi_m + \delta\hat{\psi}_m. \tag{2.33}$$

Here, ψ_m is the mean field ground state order parameter and $\delta\hat{\psi}_m$ is the weak perturbations to this state.$\hat{\psi}_m$ is the field order of the perturbed state in the flat potential limit. $\hat{\psi}_m$ can be expanded in terms of plane waves as:

$$\hat{\psi}_m = \frac{1}{\Omega}\sum_k \hat{a}_{k,m} e^{ik.r} \tag{2.34}$$

We use this wave operator in the second quantized Hamiltonian of the spinor BEC. The condensate is considered to be in the $k = 0$ state. We expand the Hamiltonian upto a second order in $a_{k\neq\hat{0},m}$, where $a_{\hat{k},m}$ is the is the annihilation operator of a boson with wavevector k

and Ω is the volume of the system. By doing so we get the Hamiltonian represented by $\hat{H}_B$

$$\begin{aligned}\hat{H}_B &= E_0+\frac{D_{corr}}{4\varepsilon_k}+\sum_{k\neq 0,m}(\varepsilon_k-pm+qm^2-\mu)\hat{a}^\dagger_{k,m}\hat{a}_{k,m}\\ &+\frac{N}{\Omega}\sum_{k\neq 0}\sum_{m_1,m_2,m_1^{'},m_2^{'}}(C^{m_1m_2^{'}}_{m_1^{'}m_2}+C^{m_1m_2^{'}}_{m_2m_1^{'}})\psi_{m_1^{'}}\psi^*_{m_2^{'}}\hat{a}^\dagger_{k,m_1}\hat{a}_{k,m_2}\\ &+\frac{N}{2\Omega}\sum_{k\neq 0}\sum_{m_1,m_2,m_1^{'},m_2^{'}}C^{m_1m_2}_{m_1^{'}m_2^{'}}(\psi^*_{m_1}\psi^*_{m_2}\hat{a}_{-k,m_2^{'}}\hat{a}_{k,m_1^{'}}\\ &+\psi_{m_1^{'}}\psi_{m_2^{'}}\hat{a}^\dagger_{-k,m_2}\hat{a}^\dagger_{k,m_1})\end{aligned} \tag{2.35}$$

In the previous equation,

$$\begin{aligned}E_0 &= N[\sum_m(-pm+qm^2)\,|\psi_m|^2\\ &+\frac{N(N-1)}{\Omega^2}\sum_{m_1,m_2,m_1^{'},m_2^{'}}\psi^*_{m_1}\psi^*_{m_2}\psi_{m_2^{'}}\psi_{m_1^{'}}]\end{aligned} \tag{2.36}$$

$$D_{corr} = \frac{N(N-1)}{\Omega^2}C^{m_1m_2}_{m_1^{'}m_2^{'}}\psi^*_{m_1}\psi^*_{m_2}\psi_{m_2^{'}}\psi_{m_1^{'}} \tag{2.37}$$

The first two terms in the Hamiltonian correspond to the condensate that is in $k=0$ state.The rest of the terms in the Hamiltonian are due the fluctuations in the condensate for which $k\neq 0$ and the resulting dynamics.

$$\begin{aligned}C^{m_1^{'}m_2^{'}}_{m_1m_2} &= (c_0^2+2c_1^2)\delta_{m_1m_1^{'}}\delta_{m_2m_2^{'}}\\ &+c_1(2c_0-c_1)\sum_{\rho=x,y,z}(f_\rho)_{m_1m_1^{'}}(f_\rho)_{m_2m_2^{'}}\end{aligned} \tag{2.38}$$

ε_k in the Hamiltonian is the kinetic energy of the boson for which $k\neq 0$, Ω is the volume of the condensate while $\hat{a}_{k,m}$ is the annihilation operator of the boson of spin-'m' and momentum-'k' and ψ_m is the order parameter.This Hamiltonian can be written in a $(2f+1)\times(2f+1)$matrix form. For spin-1 BEC it is a 6×6 matrix given below:

$$\begin{aligned}\hat{H}_B &= E_0-\frac{1}{2}\sum_{k\neq 0}Tr[\mathbf{H^0_k}+\mathbf{H^{(1)}}]-\frac{D_{corr}}{2\varepsilon_k}+\frac{1}{2}\sum_{k\neq 0}\begin{pmatrix}\hat{\bar{\mathbf{a}}}^\dagger_k & \hat{\bar{\mathbf{a}}}_k\end{pmatrix}\\ &\begin{bmatrix}\mathbf{H^0_k}+\mathbf{H^{(1)}} & \mathbf{H^{(2)}}\\ [\mathbf{H^{(2)}}]^* & [\mathbf{H^0_k}+\mathbf{H^{(1)}}]^*\end{bmatrix}\begin{pmatrix}\hat{\mathbf{a}}_k\\ \hat{\mathbf{a}}^\dagger_k\end{pmatrix}\end{aligned} \tag{2.39}$$

Here, H_k^0, $H^{(1)}$ are Hermitian matrices and $H^{(2)}$ is a symmetric matrix and $\hat{\mathbf{a}}_k$, $\mathbf{a}_k^\dagger$ are annihilation and creation operator vectors.They are defined as,

$$\mathbf{H_k^{(0)}} = (\varepsilon_k - \mu)\mathbf{1} - pf_z + qf_z^2 \tag{2.40}$$

$$H^{(1)}_{m_1 m_2} = \frac{N}{\Omega}\sum_{m_1' m_2'} (C^{m_1 m_2'}_{m_1' m_2} + C^{m_1 m_2'}_{m_2 m_1'})\psi_{m_1'}\psi^*_{m_2'} \tag{2.41}$$

$$H^{(2)}_{m_1 m_2} = \frac{N}{\Omega}\sum_{m_1' m_2'} C^{m_1 m_2}_{m_1' m_2'}\psi_{m_1'}\psi_{m_2'} \tag{2.42}$$

$$\hat{\mathbf{a}}_k = \begin{pmatrix} \hat{a}_{k,1} \\ \hat{a}_{k,0} \\ \hat{a}_{k,-1} \end{pmatrix} \hat{\mathbf{a}}_k^\dagger = \begin{pmatrix} \hat{a}^\dagger_{k,1} \\ \hat{a}^\dagger_{k,0} \\ \hat{a}^\dagger_{k,-1} \end{pmatrix} \tag{2.43}$$

This Hamiltonian is diagonalized using Bogoliubov-de Gennes transformations which are linear transformation that couple the creation and annihilation operators of the Bose-Einstein condensate while still retaining the statistics of Bosons.

$$\begin{pmatrix} \hat{\mathbf{a}}_k \\ \hat{\mathbf{a}}^\dagger_{-k} \end{pmatrix} = \begin{bmatrix} \hat{\mathbf{U}}_k & \hat{\mathbf{V}}^*_{-k} \\ \hat{\mathbf{V}}_k & \hat{\mathbf{U}}^*_{-k} \end{bmatrix} \begin{pmatrix} \hat{\mathbf{b}}_k \\ \hat{\mathbf{b}}^\dagger_{-k} \end{pmatrix} \tag{2.44}$$

$$(\hat{\mathbf{U}}_k\hat{\mathbf{U}}_k^\dagger - \hat{\mathbf{V}}^*_{-k}\hat{\mathbf{V}}^T_{-k})_{mm'} = \delta_{mm'} \tag{2.45}$$

$$(\hat{\mathbf{U}}_k\hat{\mathbf{V}}_k^\dagger - \hat{\mathbf{V}}^*_{-k}\hat{\mathbf{U}}^T_{-k})_{mm'} = 0 \tag{2.46}$$

This transforms the Hamiltonian of interacting real particles to a Hamiltonian of non-interacting quasi-particles with dispersion relation $\varepsilon(k)$. The real particle is a superposition of forward and backward propagating quasi-particle. Also, the resulting Bogoliubov equation is an eigenvalue equation for a non-Hermitian matrix and may have complex eigenvalues giving rise to a dynamic instability. The solution for a given phase gives us three modes, a density mode and two other spin modes. The energy spectra is obtained for the different ground state phases of the spin-1 BEC given in Table-2.2 and it also is summarized in [35]

2.5 Bogoliubov Excitations in Spin-1 BEC

Bogoliubov Hamiltonian in a spin system has more than one mode.The density mode is the mode corresponding to the populated components.It is listed first in Table-2.2. Collective

Phase	Energy spectra	Quasi particle ($\hat{b}_{k,m}$)
F	$\sqrt{\varepsilon_k[\varepsilon_k+2(c_0+c_1)n]}$	$\mathrm{sgn}(c_0+c_1)\sqrt{\frac{\varepsilon_k+(c_0+c_1)n+E_{k,1}}{2E_{k,1}}}\hat{a}_{k,1}$ $+\sqrt{\frac{\varepsilon_k+(c_0+c_1)n-E_{k,1}}{2E_{k,1}}}\hat{a}^\dagger_{-k,1}$
	ε_k+p-q	$\hat{a}_{k,0}$
	$\varepsilon_k+2p-2c_1n$	$\hat{a}_{k,-1}$
P	$\sqrt{\varepsilon_k[\varepsilon_k+2c_0n]}$	$\mathrm{sgn}(c_0)\sqrt{\frac{\varepsilon_k+c_0n+E_{k,0}}{2E_{k,0}}}\hat{a}_{k,0}$ $+\sqrt{\frac{\varepsilon_k+c_0n-E_{k,0}}{2E_{k,0}}}\hat{a}^\dagger_{-k,0}$
	$\sqrt{(\varepsilon_k+q)(\varepsilon_k+q+2c_1n)}\pm p$	$\mathrm{sgn}(c_1)\sqrt{\frac{\varepsilon_k+q+c_1n+(E_{k,\pm}\pm p)}{2(E_{k,\pm}\pm p)}}\hat{a}_{k,\pm}$ $+\sqrt{\frac{\varepsilon_k+q+c_1n-(E_{k,\pm}\pm p)}{2(E_{k,\pm}\pm p)}}\hat{a}^\dagger_{-k,\mp}$
AF	$\sqrt{(\varepsilon_k-q)^2+2c_1n(\varepsilon_k-q)+c_1^2f_z^2}$	$\mathrm{sgn}(c_1)\sqrt{\frac{\varepsilon_k-q+c_1n+E_{k,0}}{2E_{k,0}}}\hat{a}_{k,0}$ $+\sqrt{\frac{\varepsilon_k-q+c_1n-E_{k,0}}{2E_{k,0}}}\hat{a}^\dagger_{-k,0}$
	$\sqrt{\varepsilon_k[\varepsilon_k+c_0+c_1+\Upsilon]}$ $\Upsilon=\sqrt{(c_0-c_1)^2+4c_0c_1f_z^2}$	$\mathrm{sgn}(c_0)\sqrt{\frac{\varepsilon_k+c_0n+E_{k,1}}{2E_{k,1}}}(\frac{\hat{a}_{k,1}+\hat{a}_{k,-1}}{\sqrt{2}})$ $+\sqrt{\frac{\varepsilon_k+c_0n-E_{k,1}}{2E_{k,1}}}(\frac{\hat{a}_{k,1}+\hat{a}_{-k,-1}}{\sqrt{2}})$
	$\sqrt{\varepsilon_k[\varepsilon_k+c_0+c_1-\Upsilon]}$	$\mathrm{sgn}(c_1)\sqrt{\frac{\varepsilon_k+c_1n+E_{k,-1}}{2E_{k,-1}}}(\frac{\hat{a}_{k,1}-\hat{a}_{k,-1}}{\sqrt{2}})$ $+\sqrt{\frac{\varepsilon_k+c_1n-E_{k,-1}}{2E_{k,-1}}}(\frac{\hat{a}_{k,1}-\hat{a}_{-k,-1}}{\sqrt{2}})$
BA	$\sqrt{\varepsilon_k[\varepsilon_k+q]}$	$\mathrm{sgn}(q)\sqrt{\frac{\varepsilon_k+q/2+E_{k,0}}{2E_{k,0}}}(\frac{\hat{a}_{k,1}-\hat{a}_{k,-1}}{\sqrt{2}})$ $+\sqrt{\frac{\varepsilon_k+q/2-E_{k,0}}{2E_{k,0}}}(\frac{\hat{a}_{k,1}-\hat{a}_{-k,-1}}{\sqrt{2}})$
	$\sqrt{\varepsilon_k^2+(c_0-c_1)n\varepsilon_k+2(c_1n)^2(1-q^2)\pm\Lambda_k}$ $\Lambda_k=\sqrt{[(c_0+3c_1)n\varepsilon_k+\Gamma_k}$ $\Gamma_k = 2(c_1n)^2(1-q^2)] - 4c_1(c_0+2c_1)(nq\varepsilon_k)^2$	

Table 2.2 Energy spectra and quasi-particle excitations of ferromagnetic, antiferromagnetic, polar and broken-axis symmetric phases of spin-1 BEC

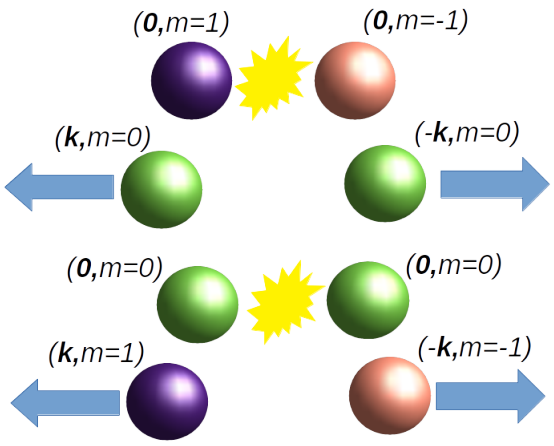

Fig. 2.3 Elementary excitations in a Spin-1 BEC that help populate the spin modes.

excitation in this mode shows phonon like excitations for large wavelengths and particle like excitations for large wavelengths.

The spin mode corresponds to the last two modes listed in the Table-2.2. The transfer of population to these spin modes rests on the elementary excitations which conserves spin. In case of Spin-1 BEC there exists only two such excitations shown in figure 2.3. These excitations creates fluctuation in the F_x and F_y. Fluctuations in F_x and F_y create interesting spin-textures which we can carry out further study on.

As has been established earlier, one can study elementary excitations in BEC by periodically driving the system. Periodic driving of the s-wave scattering length or trap parameter gives rise to Faraday patterns which have wave number indicative of the Bogoliubov mode resonant with half the driving frequency. Since, collective excitations in spin-1 BEC have spin modes which can create intricate spin-textures it would serve us well to study them.

To this end we first carry out a brief study of pattern formation and linear stability analysis which will help us in exploring the system described so far.

2.6 Pattern Formation

We observe patterns in systems all around us varying from stripes on wind-swept sands to intricate patterns of snowflakes to the complex patterns in weather and living systems[36].Pattern formations in nonlinear dynamical systems and in context of phase transitions has been of particular interest.Intricate spatial or temporal patterns emerge from relatively simple systems when there are instabilities created in the system as a result of some perturbation.Understanding the the concept of instability is central to understanding pattern forma-

tion.Any system with an instability will deform by large amounts in response to infinitesimally small perturbations.Non-linearity in the system which moves the unstable system to the new state is another crucial component for pattern formation [37].

2.6.1 Linear Stability Analysis for pattern formation

The pattern forming tendencies of a nonequilibrium system is classified using linear stability analysis. Most patterns develops from a state that has no spatial structure- the uniform state. A uniform system is defined mathematically as a system which is translational symmetry i.e on infitesimal translation in any direction $x \to x + x_0$ the system remains invariant. Nonequilibrium systems such as a periodically driven nonlinear system cannot have complete translational symmetry as gradients of energy, momentum or matter develop on being driven which move the system away from equilibrium towards pattern formation. Thus uniform nonequilibrium states serve as an appropriate starting point for a stability analysis of a pattern forming system.

The procedure for linear stability analysis starting from a uniform non-equilibrium state is outlined below[38]:

- The equations describing the dynamics of the system is first obtained.
- To simplify calculations periodic or infinite boundaries are considered.
- A uniform time-independent solution to the system being considered is found

$$u(x) = u_h \tag{2.47}$$

- Perturbations to this uniform system is considered to be both spatially and temporally dependent and of the form

$$u(x) = u_h + u_p(x,t) \tag{2.48}$$

- The equations describing the dynamics of the system are then linearized with respect to the perurbations.
- A general solution for the perturbed part can be taken as

$$u_p(x,t) = \sum_k c_k e^{\sigma_k t} e^{ikx} \tag{2.49}$$

  Here, coefficients c_k and exponent σ_k are complex numbers and k is the wave number corresponding to them.

- The uniform system is stable if $Re(\sigma_k) = 0$ for all wavenumbers.
- Pattern formation is observed in the system if $Re(\sigma_k) > 0$ for any particular 'k' and that perturbation grows exponentially in time.
- The wave number of the pattern correspond to the wavenumber with $max(Re(\sigma_k))$

2.7 Faraday Patterns

A nonequilibrium pattern-forming system to which linear stability analysis can be successfully applied to study pattern formation is the Faraday experiment.

The Faraday experiment comprises of vertical vibrations of a thin film of a fluid. This gives rise to non-linear standing waves called Faraday waves when the driving frequency is greater than a critical value.The waves form intricate patterns ranging from lattices of stripes to lattices of squares, and hexagons.Michael Faraday was the first to study and report the findings of such a system in 1831.

The size and symmetry of these patterns is an indicator of the viscosity and surface tension properties of the fluid. Similar pattern formation can be used to study elementary excitation in Bose-Einstein Condensates. The specifics of how this is done is discussed in the following sections.

2.8 Faraday Patterns in Bose-Einstein Condensates

The analogue of forcing the surface of the fluid up and down in the Faraday experiment is the periodic modulation of the interatomic s-wave scattering length, a variable that describes the range of the interatomic forces, of the condensate. This leads to excitations of the sub-harmonic patterns in the atomic density through a parametric resonance resonance. The dominant wavelength of the instability and the symmetries of the selected patterns are intrinsic properties of the system,independent of (or only weakly dependent on the initial or boundary conditions).

Faraday patterns in periodically driven Bose-Einstein condensates (BECs) have been studied extensively in various trapping geometries in both scalar [17, 39, 40, 18, 41–47] and multicomponent condensates [48–51]. It has also been implemented experimentally for a scalar BEC in a cigar shaped trap[39].

We review the studies on Faraday patterns in scalar BECs and Scalar Dipolar BECs.

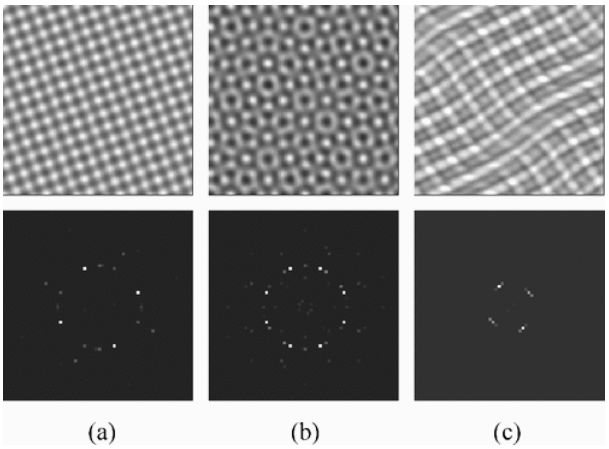

Fig. 2.4 Faraday Patterns in scalar BEC for different driving frequencies.(Taken from Figure 3. in Phys. Rev. Lett. 89, 210406)

2.8.1 Faraday Patterns in Scalar BEC

Faraday patterns in scalar BEC was reported in [17]. It outlined how patterns formed on modulation of s-wave scattering length in a BEC was simlar to the Faraday waves in vertically perturbed classical fluids.

The pattern size was determined by the Bogoliubov mode resonant with half the driving frequency much like classical fluids where standing waves which oscillate at half the driving frequency appear on vertical temporal perturbation.

Linear stability analysis is used to provide insight into pattern formation in this system. The mean-field equation (or the Gross-Pitaveskii equation) that describes the dynamics of the system is given as,

$$i\frac{d\psi}{dt} = \nabla^2\psi + V(r)\psi + c\,|\psi|^2\,\psi \tag{2.50}$$

Here, ψ is the order parameter of the scalar BEC,$V(r)$ is the trap potential and $c = \frac{4\pi\hbar^2 a}{M}$ represents the magnitude of interactions between the bosons. c depends upon the s-wave scattering a length which is modulated in time as,

$$a \to a(t) = a[1 + 2\alpha\cos(2\omega t)] \tag{2.51}$$

The modulated state can be given as a sum of uniform and perturbed state.

$$\Psi = \Psi_{homg} + \Psi_{homg} w(t)\cos(\vec{k}.\vec{r}) \tag{2.52}$$

where $w(t) = u(t) + iv(t)$ is the complex amplitude of the spatial perturbation. We solve for the real amplitude of the spatial perturbations.

$$\frac{d^2u}{dt^2} + [\Omega^2(\vec{k}) + 4c_0k^2\alpha\cos(2\omega t)]u = 0 \tag{2.53}$$

$$\Omega(\vec{k}) = \sqrt{k^2[k^2 + 2c_0]} \tag{2.54}$$

The solution to the equation describing the dynamics of the amplitude of spatial perturbation is a Mathieu equation. The solution to the Mathieu equation is of the form:

$$u(t) = A(t)e^{\sigma t} \tag{2.55}$$

where, σ is complex. The solution creates an instability which grows with time causing the system to lose translational symmetry. The nonlinearity in the system drives the system away from the uniform state.

2.8.2 Faraday Patterns in Scalar Dipolar BEC

Faraday Patterns in scalar BEC with dipolar interactions is much more interesting. The Bogoliubov excitation of a dipolar BEC has a roton-maxon excitation spectrum [18].

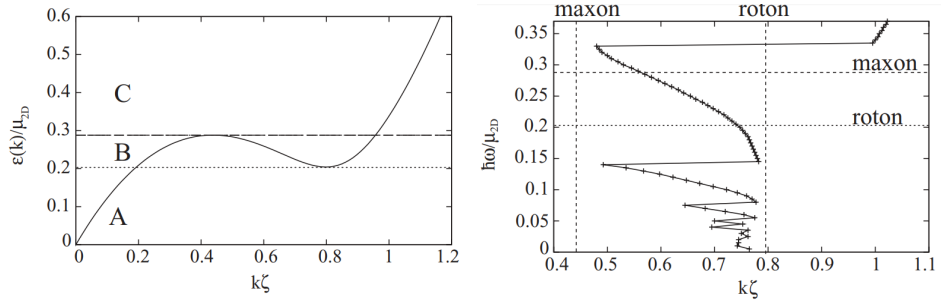

(a) (b)

Fig. 2.5 (a) Dispersion of a 2D scalar dipolar BEC.(b) Most unstable k as a function of ω for scalar dipolar BEC. (Taken from Fig-1 and Fig-4 of Phys. Rev. A 81, 033626)

In the case of a scalar BEC without dipolar interaction the wave number "k" increases monotonously with driving frequency whereas as wavenumber selection is much more involved in scalar BEC with dipolar interactions since for a single driving frequency multiple "k" values are resonant. The "k" selected has the largest value of $Re(\sigma)$.

This selection is again not trivial and abrupt changes in pattern size are seen as indicated by the relation between unstable "k" as a function of ω.

2.8.3 Faraday Patterns in Spin-1 Spinor BEC

We explore Faraday patterns in homogeneous Quasi-2D Spin-1 BEC. Patterns with wave number indicative of the Bogoliubov mode resonant with half the driving frequency emerge in the Q2D spin-1 spinor condensate on periodic modulation of the scattering lengths. The details of Q2D system is presented in Appendix. A consequence of the spin-degrees of freedom is that the Bogoliubov modes in a Spin-1 BEC are multi-branched with both spin and density modes or coupled between them. Since there are multiple modes which can be excited at the same time we observe not only density patterns as reported in scalar BEC but also spin dynamics and interesting spin-textures.

Another consequence of the spin-degree of freedom is that there are two s-wave scattering length channels one with total spin $F = 0$ and the other with total spin $F = 2$ which we can modulate independently or together. Periodic temporal modulation of these channel may be achieved by magnetic or optical Feshbach resonances[29] or by applying radio frequency or microwave fields[25–28]. We consider three scenarios for time modulated scattering lengths:

- a_0 is temporally modulated and a_2 is held constant
- a_0 constant and a_2 is temporally modulated
- a_0 and a_2 are temporally modulated

We also have to consider another parameter which influences the dynamics of the system - c_1, which is the magnitude of the interaction between the spins. The spin-dependent interaction between two bosons with spins, F_1 and F_2 is given as $c_1 F_1 \cdot F_2$.

- **Antiferromagnetic interactions** $c_1 > 0$- interactions between the bosons is repulsive.We consider a BEC with atomic Na-23 which has antiferromagnetic interactions between its atoms.
- **Ferromagnetic interactions** $c_1 < 0$- interactions between the bosons is attractive.We consider a BEC with atomic Rb-87 which has ferromagnetic interactions between its atoms.

The difference in the kind of interactions between the atoms is also reflected in the ground state phases of the spinor-condensate.The different ground state phases for the two cases is listed in Table-2.1 and phase diagram below. We consider the three different kinds of periodic modulation listed above for the system in each of these ground states. The values of different parameters that have been used in the numerical evaluations are listed in the Appendix. We analyse the dynamics of this periodically modulated system both analytically

as well as numerically using the theory explained in previous section and the algorithm in [52].

Chapter 3

Results and Discussions-I

3.1 Periodic modulation of the a_0 scattering channel

The $F = 0$ scattering channel is modulated with amplitude α and frequency ω.

$$\tilde{a_0} = \tilde{a_0} + \tilde{a_0}(2\alpha\cos(2\omega t)) \tag{3.1}$$

The spin dependent and the spin independent interactions can then be written as:

$$\tilde{c_0} = c_0 + \tilde{a_0}(2\alpha\cos(2\omega t)) \tag{3.2}$$

$$\tilde{c_1} = c_1 - \tilde{a_0}(2\alpha\cos(2\omega t)) \tag{3.3}$$

Here, $c_0 = \frac{4\pi(a_0+2a_2)\hbar^2}{3M}$ is the magnitude of the spin independent interaction between the atoms and $c_1 = \frac{4\pi(a_2-a_0)\hbar^2}{3M}$ is the strength of the spin-spin interaction between the atoms and $\tilde{a_0} = \frac{4\pi a_0\hbar^2}{3M}$. The modulation results in a spatially homogenous temporally modulated solution.

$$\Psi e^{[-i\mu t + \frac{\alpha\tilde{a_0}}{\omega}\sin(2\omega t)]} \tag{3.4}$$

Here, $\Psi = (\psi_+, \psi_0, \psi_-)$ is the spatially homogenous order parameter . A dynamical instability may arise in this system as a result of this modulation. We perform a linear stability analysis of this uniform state against a spatially and temporally modulated state.

$$(\Psi + \mathbf{w}\cos(\vec{k}.\vec{r}))e^{[-i\mu t + \frac{\alpha\tilde{a_0}}{\omega}\sin(2\omega t)]} \tag{3.5}$$

Here, $\mathbf{w} = (w_+, w_0, w_-)$ is is the complex-valued amplitude of the perturbation. Linear stability analysis is performed to determine if there might occur a spontaneous spatial

symmetry breaking as a result of modulation. We find varied results when we start with different ground state phases.

3.1.1 Spin-1 BEC in Ferromagnetic Phase

Homogeneous spinor field for the ferromagnetic phase in the absence of any perturbation is given as:

$$(1,0,0)e^{-i\mu t} \tag{3.6}$$

Here,$\mu = -p+q+c_0+c_1$. We look at the dynamics of this system on periodic modulation of a_0 scattering channel. We perform linear stability analysis of this homogeneous state against a spatially modulated state. The equations below give the results of this analysis.

$$\frac{d^2u_+}{dt^2} + [k^2(k^2+2c_0+2c_1)+4k^2 \quad = \quad 0 \tag{3.7}$$

$$\frac{d^2u_0}{dt^2} + [(k^2+p-q)^2]u_0 = 0 \tag{3.8}$$

$$\frac{d^2u_-}{dt^2} + [(k^2+2p-2c_1)^2]u_- = 0 \tag{3.9}$$

We find that the uniform state is indeed stable against the spatially modulated state. The reason for this is that all collisions that occur in this phase have a total spin $F = 2$. Thus the system continues to retain the spatial symmetry despite the perturbation to the system as there are no atoms in the scattering channel a_0. This is further supported by the numerical simulations performed in the flat potential limit to test the parametric instability of the uniform state of a spin-1 BEC in the ferromagnetic phase when the interactions between spins is both antiferromagnic and ferromagnetic.

Spin-1 BEC with antiferromagnetic interactions

We see no patterns in any of the components.Also, we observe no spin-dynamics as there exists no two-body spin exchange process that conserves spin and transfer population from the $m = 1$ component to the $m = 0,-1$ components.

Spin-1 BEC with ferromagnetic interactions

We make similar observations in system with ferromagnetic interactions that is in the ferromagnetic phase. We see no patterns on formation when the a_0 scattering channel is modulated. Translational symmetry is preserved and we observe no spin-dynamics.

3.1.2 Spin-1 BEC in Antiferromagnetic Phase

Homogeneous spinor field for the antiferromagnetic phase in the absence of any perturbation is given below:

$$\left(\sqrt{\frac{1+\frac{p}{c_1}}{2}},0,\sqrt{\frac{1-\frac{p}{c_1}}{2}}\right)e^{-i\mu t} \tag{3.10}$$

Here,$\mu = q + c_0 n$. This phase is present only when the interactions between spins is antiferromagnetic in nature.To simplify our calculations we take $p = 0$. The system on temporal modulation of a_0 is given by a spatially uniform but temporally modulated solution,

$$\left(\sqrt{\frac{1}{2}},0,\sqrt{\frac{1}{2}}\right)e^{[-i\mu t+\frac{\alpha\tilde{a}_0}{\omega}\sin(2\omega t)]} \tag{3.11}$$

We perform linear stability analysis of this uniform system against a spatially modulated system one. We obtain a Mathieu equation for the spin modes and the coupled density mode.

$$\frac{\partial^2\zeta_+}{\partial t^2}+[(k^2+2c_0)k^2-k^2(2\tilde{a}_0)(2\alpha\cos(2\omega t))]\zeta_+ = 0 \tag{3.12}$$

$$\frac{\partial^2\zeta_-}{\partial t^2}+[(k^2+2c_1)k^2-k^2(2\tilde{a}_0)(2\alpha\cos(2\omega t))]\zeta_- = 0 \tag{3.13}$$

$$\frac{\partial^2 u_0}{\partial t^2}+[(k^2-q+2c_1)(k^2-q)-(k^2-q)(2\tilde{a}_0)(2\alpha\cos(2\omega t))]u_0 = 0 \tag{3.14}$$

Here, $\zeta_+ = u_+ + u_-$ and $\zeta_- = u_+ - u_-$.

Solution to these equations is obtained using the Floquet theorem [53]. The Floquet exponent $\sigma_m = \sigma_m(\omega,\alpha,k)$ determines the stability of these solutions. The system is unstable if $Re(\sigma_m) > 0$. The presence of three floquet exponents makes this system different from the scalar BEC in which a single floquet exponent determines the stability of the system. On solving the two Mathieu equations we make the following observations:

- Both the density and spin modes are rendered unstable on periodic driving of the a_0 scattering channel.
- $\sigma_0 > \sigma_\pm$
  - For $\omega = \frac{\pi}{2}$, the floquet exponent corresponding to most unstable k of each mode are compared i.e, $\sigma_+ = 0.0625$-density mode,$\sigma_- = 0.495733$-spin mode $< \sigma_0 = 0.495734$-spin mode

  - For $\omega = \pi$, the floquet exponent corresponding to most unstable k of each mode are compared i.e, $\sigma_+ = 0.060545$-density mode,$\sigma_- = 0.273984$-spin mode $<$ $\sigma_0 = 0.273986$-spin mode

- This implies that one of the spin mode is the most unstable and will grow faster than the others.

Unlike the ferromagnetic phase, there exists two-body spin exchange process that conserves spin and can transfer population from the $m = \pm 1$ components to the $m = 0$ component and vice versa. Thus on modulation of a_0 scattering channel we expect translational symmetry breaking and spin-dynamics. Numerical simulations were performed to study this system.

Spin-1 BEC with antiferromagnetic interactions

We performed numerical simulations with two different driving frequencies.

The real and momentum space distribution is given in figure [3.1] ,spin-textures and spin dynamics are shown in the figures [3.2] and [3.3]. Patterns were seen in both real and momentum space on periodic modulation of the a_0 scattering channel.

One observation we make when the spin-mode is the most unstable mode is that several frequencies are unstable at the same time in the collective system allowing no discernible symmetry in the pattern formed.

The reason for this is that the ground state of the system corresponds to the system being in the $m = \pm 1$ component while the modulation seeks to transfer the population to $m = 0$ mode. The system tries to restore the population to the $m = \pm 1$ components via the process outlined below:

$$(k_1, 0) + (k_2, 0) \rightarrow (k_3, 1) + (k_4, -1) \tag{3.15}$$

$$|k_1| = |k_2| = k \tag{3.16}$$

This implies that the bosons transferred from the $m = 0$ component to the $m = \pm 1$ components will have the momenta in the range,

$$-2k < (k_3, k_4) < 2k \tag{3.17}$$

This coincides with the numerical results.The growth of the $m = 0$ component due to the instability must be much larger than the rate of transfer of population back to $m = \pm 1$ components initially. This is evident in the spin-dynamics which shows rapid growth of the $m = 0$ component with time initially.

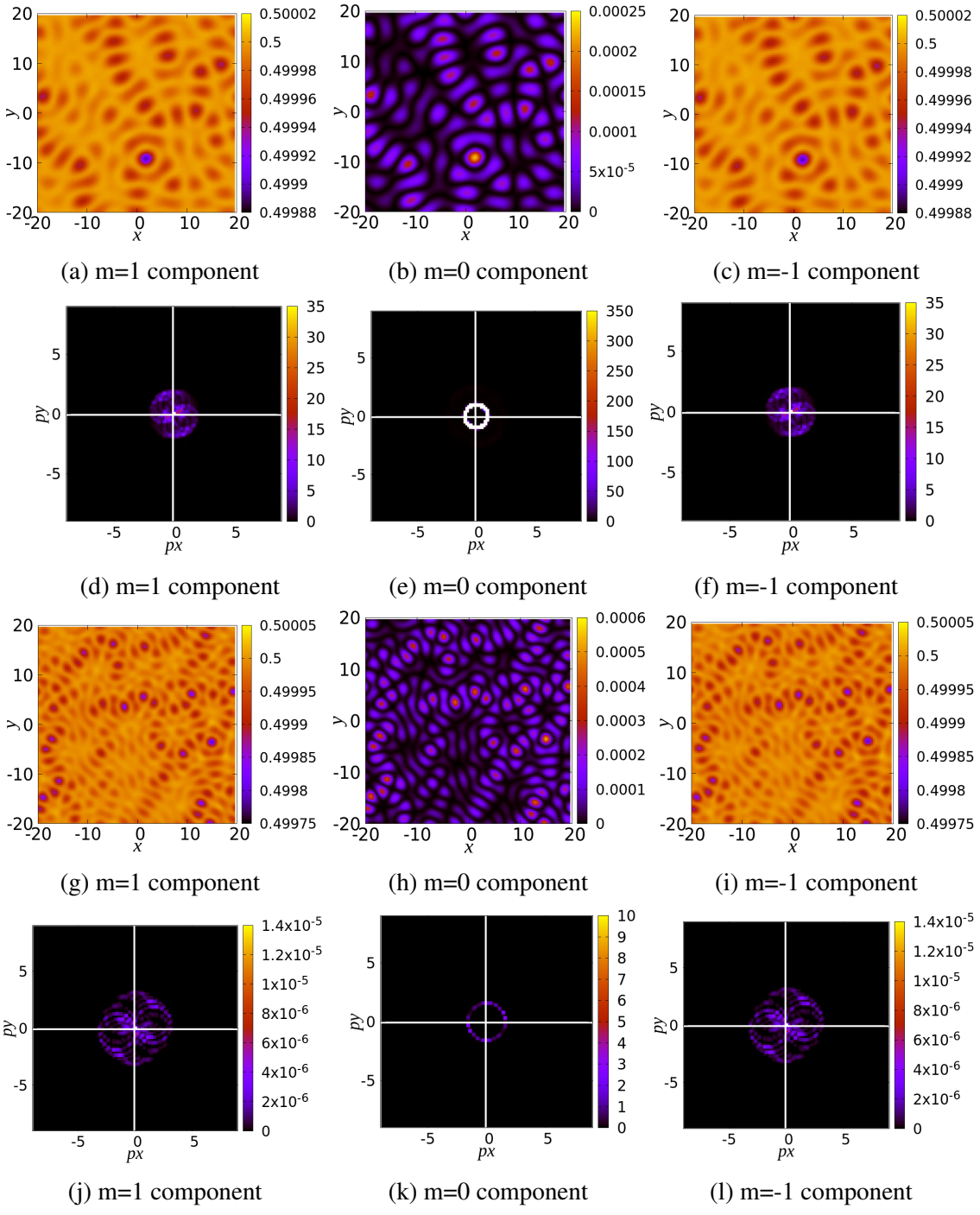

Fig. 3.1 Real and momentum space distribution of the different components of the AFM phase of a spin-1 BEC on periodic modulation of a_0 scattering channel with amplitude $\alpha = 0.2$ and for frequencies $\omega = \pi/2$ (above) and $\omega = \pi$ (below). The system shows patterns whose wavenumber increases with increasing modulation frequency. Here, the wavenumber of the $m = 0$ component corresponding to the most unstable mode is $k_0 = 1.044$ and $k_0 = 1.64$ which compares well with the expected $k_0 = 0.993$ and $k = 1.598$. The values of wavenumbers excited in the density mode are in the range of $-2k_0 < k_\pm < 2k_0$.

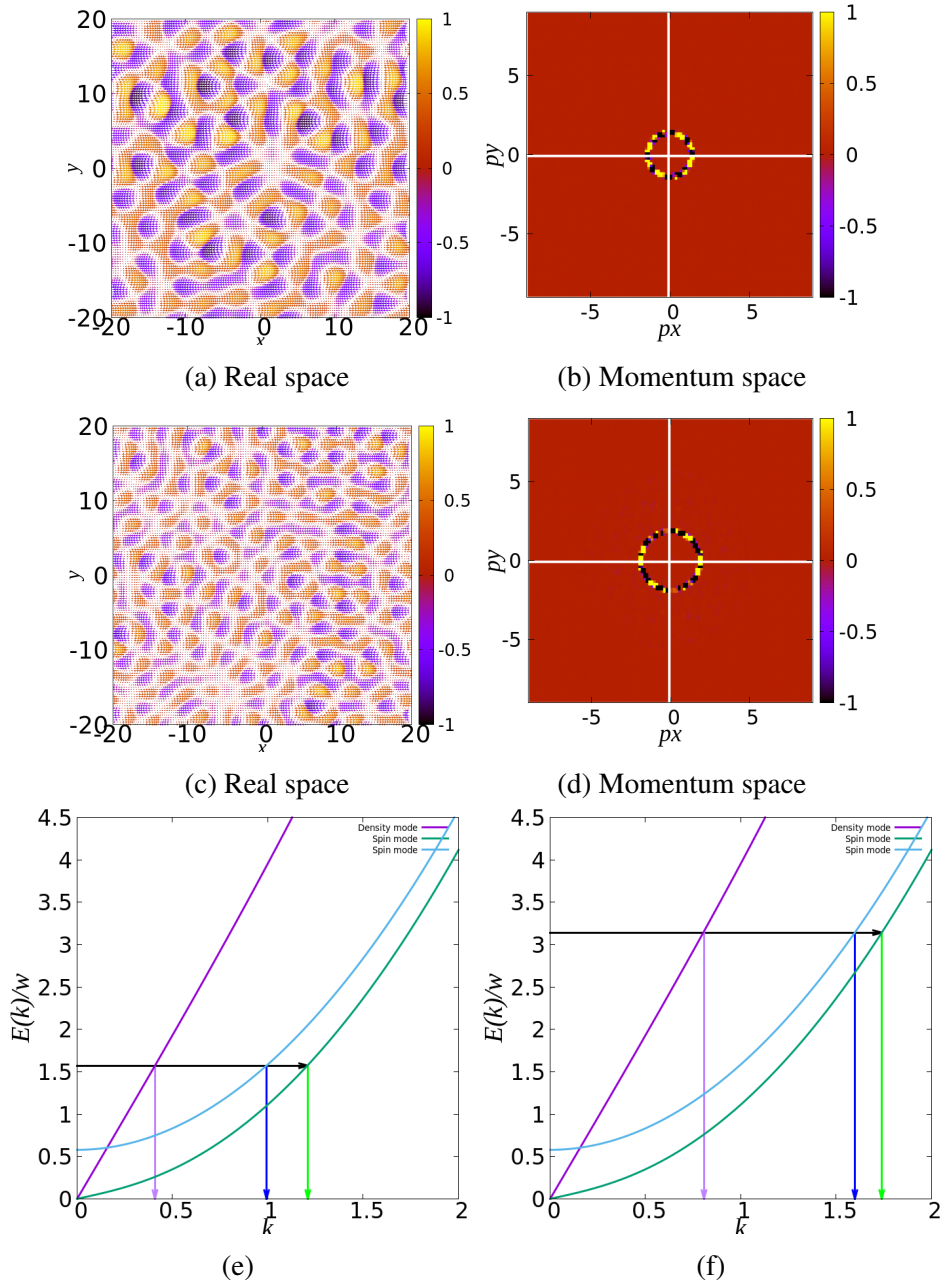

Fig. 3.2 Distribution of spins in real and momentum space for the AF phase of spin-1 BEC on periodic modulation of a_0 scattering channel with amplitude $\alpha = 0.2$ and for frequencies $\omega = \pi/2$ (above) and $\omega = \pi$ (below). The system shows patterns whose wavenumber increases with increasing modulation frequency. Here, the wavenumber of pattens formed by spin-textures corresponding to one of the spin modes is $k = 1.33$ and $k = 1.88$ which compares well with the expected wavenumbers of the spin mode $k = 1.209$ and $k = 1.739$. Fig.(e,f) shows dispersion relations obtained on solving the Bogoliubov spectra corresponding to the AFM phase. The arrows correspond to the modulating frequency and the corresponding wavenumber.

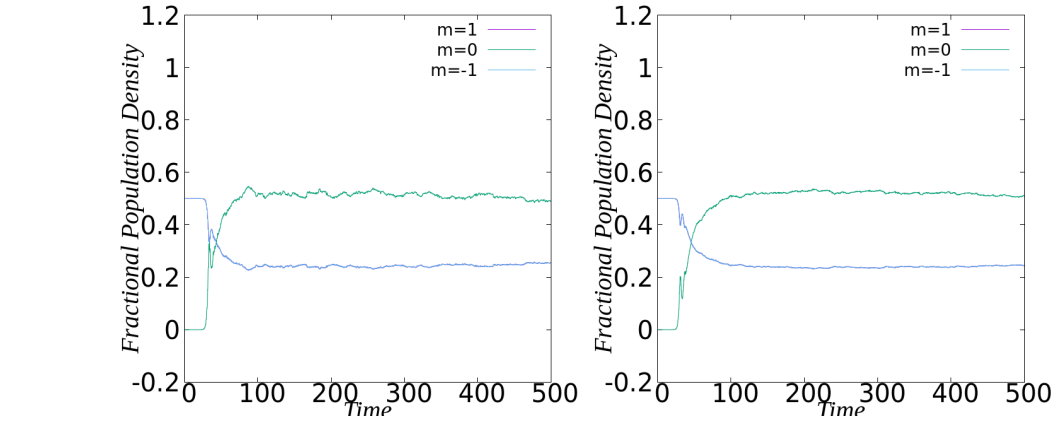

(a) Spin dynamics for $\omega = \pi/2$ (b) Spin dynamics for $\omega = \pi$

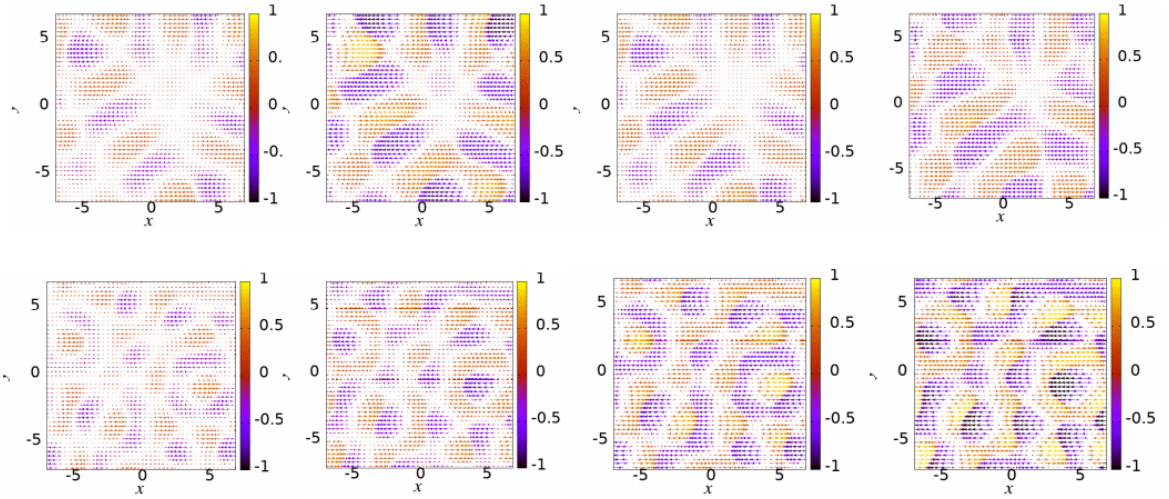

(c) Spin-textures in real space with time

Fig. 3.3 We observe flipping of directions of the spins in the spin-domains with time for both driving frequencies.

Thus we see that even though wavelength of the patterns decreases on modulation there is no particular symmetry owing to several k being excited at the same time. The wavenumber of these patterns offers us an important insight into elementary excitations of spinor BEC. In case of the antiferromagnetic phase with a_0 scattering channel alone being modulated we observe patterns with **wavenumber** indicative of the resonant **spin mode**.

3.1.3 Spin-1 BEC in Polar Phase

Homogeneous spinor field for the polar phase in the absence of any perturbation is given as:

$$(0,1,0)e^{-i\mu t} \tag{3.18}$$

Here,$\mu = c_0$. We look at the dynamics of this system on periodic modulation of a_0 scattering channel.We also consider $p = 0$ to simplify the calculations. We arrive at the equations describing the dynamics of the system using the same procedure used for the other two phases i.e, performing a linear stability analysis to test if the translational symmetry may be broken on perturbation.We arrive at the following equations for the real amplitude of spatial perturbations:

$$\frac{\partial^2\zeta_+}{\partial t^2} + (k^2+q+c_1)(k^2+q) - (k^2+q)(2\tilde{a}_0)(2\alpha\cos(2\omega t))\zeta_+ = 0 \tag{3.19}$$

$$\frac{\partial^2 u_0}{\partial t^2} + [(k^2+2c_0)k^2 - k^2(2\tilde{a}_0)(2\alpha\cos(2\omega t))]u_0 = 0 \tag{3.20}$$

Here, $\zeta_+ = u_+ + u_-$. The real amplitude of both the density mode and the coupled spin mode is described by Mathieu equations. The stability of this Mathieu equations is given by the real part of the floquet exponent of each mode. On solving the above equations we make the following observations:

- Both the density and spin modes are rendered unstable on periodic driving of the a_0 scattering channel.
- $\sigma_0 < \sigma_\pm$
  - Antiferromagnetic interactions
    - For $\omega = \frac{\pi}{2}$, the floquet exponent corresponding to most unstable k of each mode are compared i.e, $\sigma_+ = 0.0625668$-density mode $< \sigma_0 = 0.495734$-spin mode
    - For $\omega = \pi$, the floquet exponent corresponding to most unstable k of each mode are compared i.e, the floquet exponent corresponding to most unstable

k of each mode are compared i.e, $\sigma_+ = 0.060545$-density mode $< \sigma_0 = 0.273986$-spin mode

- Ferromagnetic interactions
  - For $\omega = \frac{\pi}{2}$, the floquet exponent corresponding to most unstable k of each mode are compared i.e, $\sigma_+ = 0.0659502$-density mode $< \sigma_0 = 0.428482$-spin mode
  - For $\omega = \pi$, the floquet exponent corresponding to most unstable k of each mode are compared i.e, $\sigma_+ = 0.0622128$-density mode $< \sigma_0 = 0.222552$-spin mode

- From the floquet exponents the spin mode is the most unstable and will grow faster compared to the others.

When the system is in this phase, there exists two-body spin exchange process that conserves spin and can transfer population from the $m = 0$ components to the $m = \pm 1$ components. Similar to the AFM phase on modulation of a_0 scattering channel we expect translational symmetry breaking and spin-dynamics. We performed numerical simulations to study this system for both kinds of spin interactions.

Spin-1 BEC with antiferromagnetic interactions

The results for numerical simulations are listed in Figures [3.4], [3.5] and [3.6]. Real and momentum space on periodic modulation of the a_0 scattering channel show patterns Figures [3.4]. Patterns in real space do not show have any specific symmetry as seen in the density patterns of the scalar condensate but are similar to the AF phase. Similar dynamics as described in the previous section leads to multiple wavenumbers k being excited at the same time. The modulation results in transfer of population from the $m = 0$ component to $m = \pm 1$ components which is the most unstable component.

$$(0,0) + (0,0) \rightarrow (k,1) + (-k,-1) \tag{3.21}$$

The ground state corresponds to population in the $m = 0$ component, and the system tries to restore the excited population in the $m = \pm 1$ components back to $m = 0$ component.

$$(k_1,1) + (k_2,-1) \rightarrow (k_3,0) + (k_4,0) \tag{3.22}$$

$$|k_1| = |k_2| = k \tag{3.23}$$

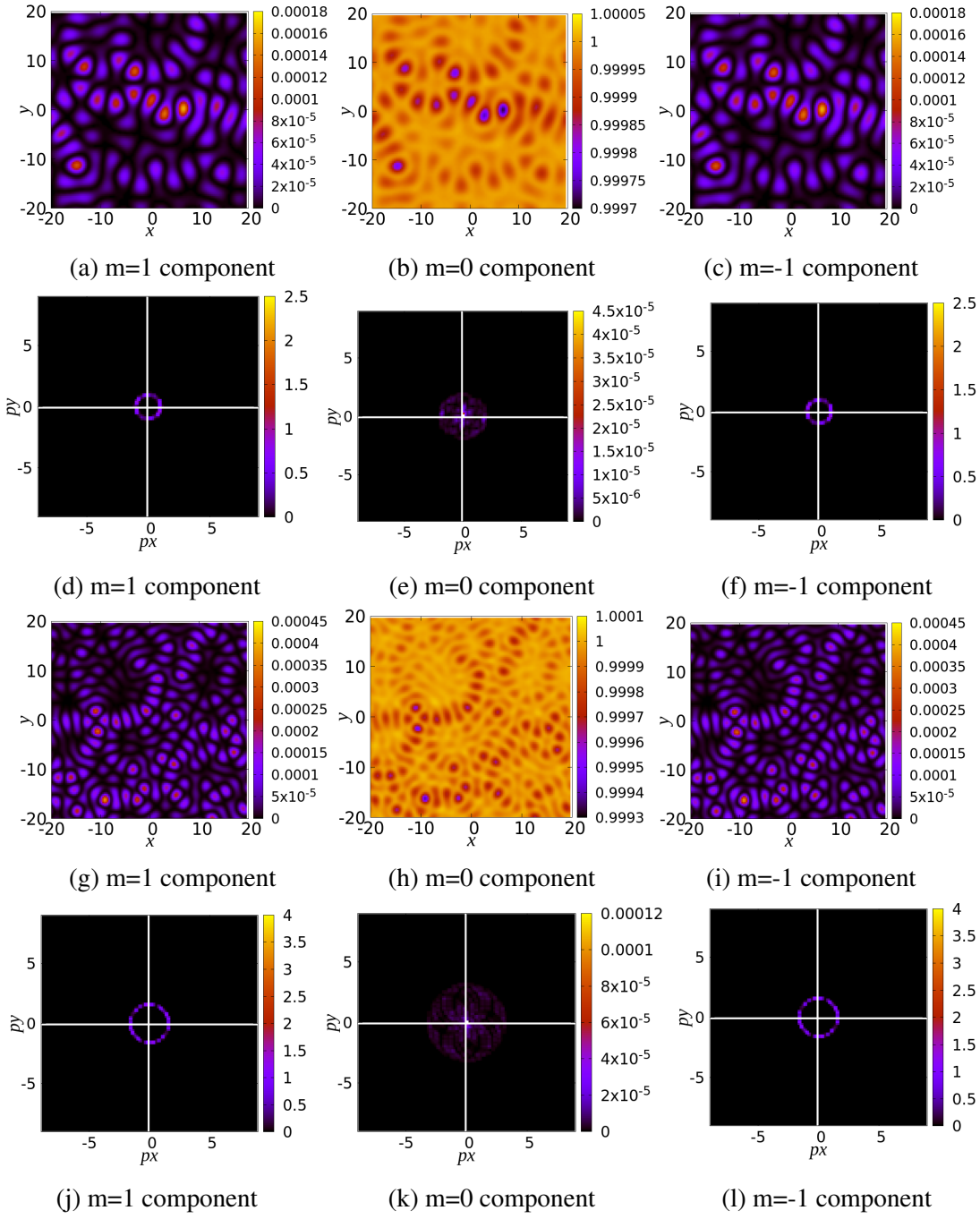

(a) m=1 component (b) m=0 component (c) m=-1 component

(d) m=1 component (e) m=0 component (f) m=-1 component

(g) m=1 component (h) m=0 component (i) m=-1 component

(j) m=1 component (k) m=0 component (l) m=-1 component

Fig. 3.4 Real and momentum space distribution of the different components of the Polar Phase spin-1 BEC with antiferromagnetic interactions on periodic modulation of a_0 scattering channel with amplitude $\alpha = 0.2$ and for frequencies $\omega = \pi/2$ (above) and $\omega = \pi$ (below). The system shows patterns whose wavenumber increases with increasing modulation frequency. Here, the wavenumber of $m = \pm 1$ components corresponding to the unstable mode is $k_\pm = 1.005$ and $k_\pm = 1.57$ which compares well with the expected $k_\pm = 0.991$ and $k_\pm = 1.6039$. The values of wavenumbers excited in the density mode are in the range of $-2k_\pm < k_0 < 2k_\pm$.

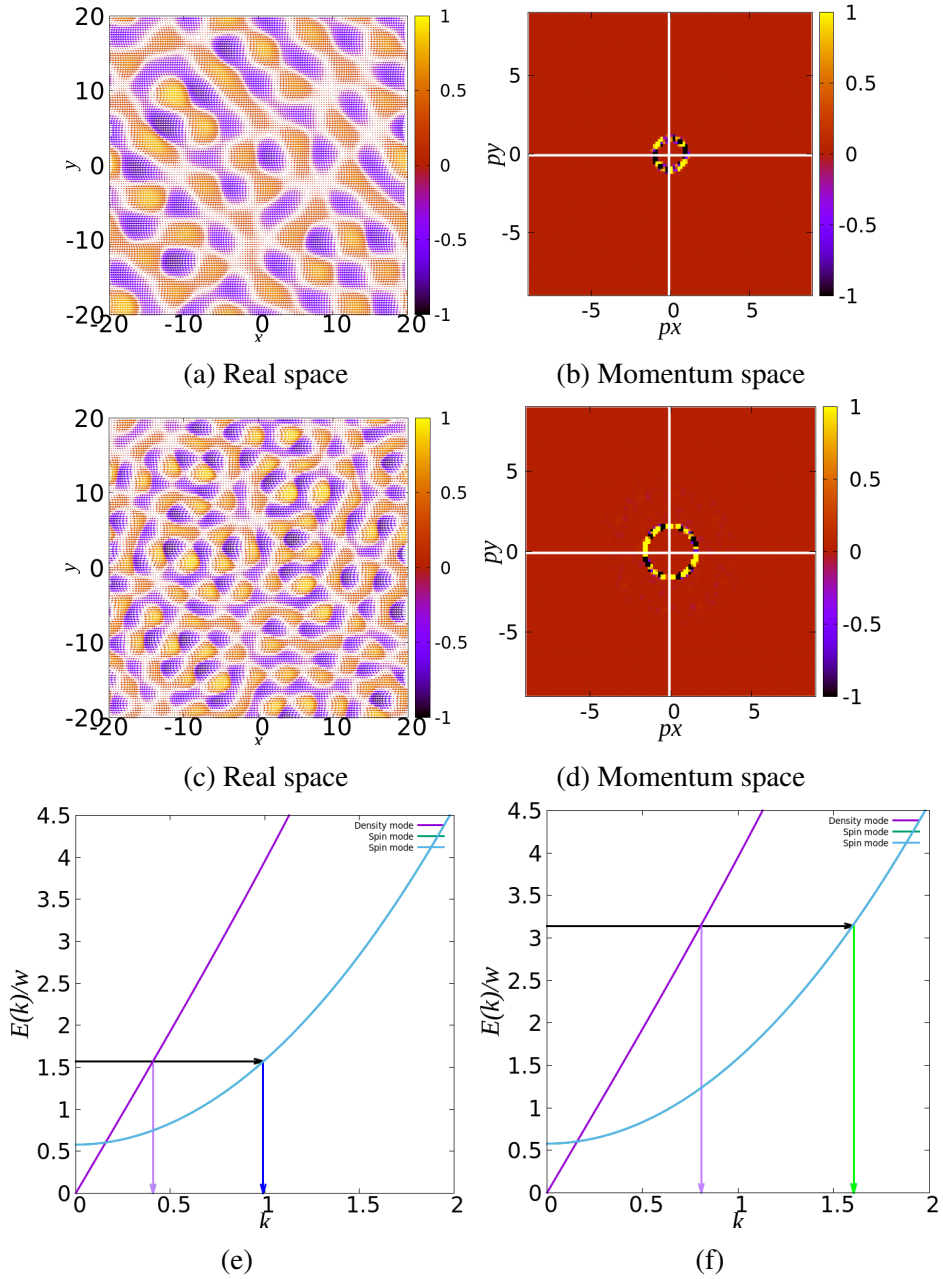

Fig. 3.5 Distribution of spins in real space for the polar phase of spin-1 BEC with antiferromagnetic interactions on periodic modulation of a_0 scattering channel with amplitude $\alpha = 0.2$ and for frequencies $\omega = \pi/2$ (above) and $\omega = \pi$ (below). Here, the wavenumber of patterns formed by spin-textures corresponding to one of the spin modes is $k = 1.01$ and $k = 1.63$ which compares well with the expected wavenumbers of the spin $k = 0.991$ and $k = 1.604$. Fig.(e,f) shows dispersion relations obtained on solving the Bogoliubov spectra corresponding to the polar phase. The arrows correspond to the modulating frequency and the corresponding wavenumber.

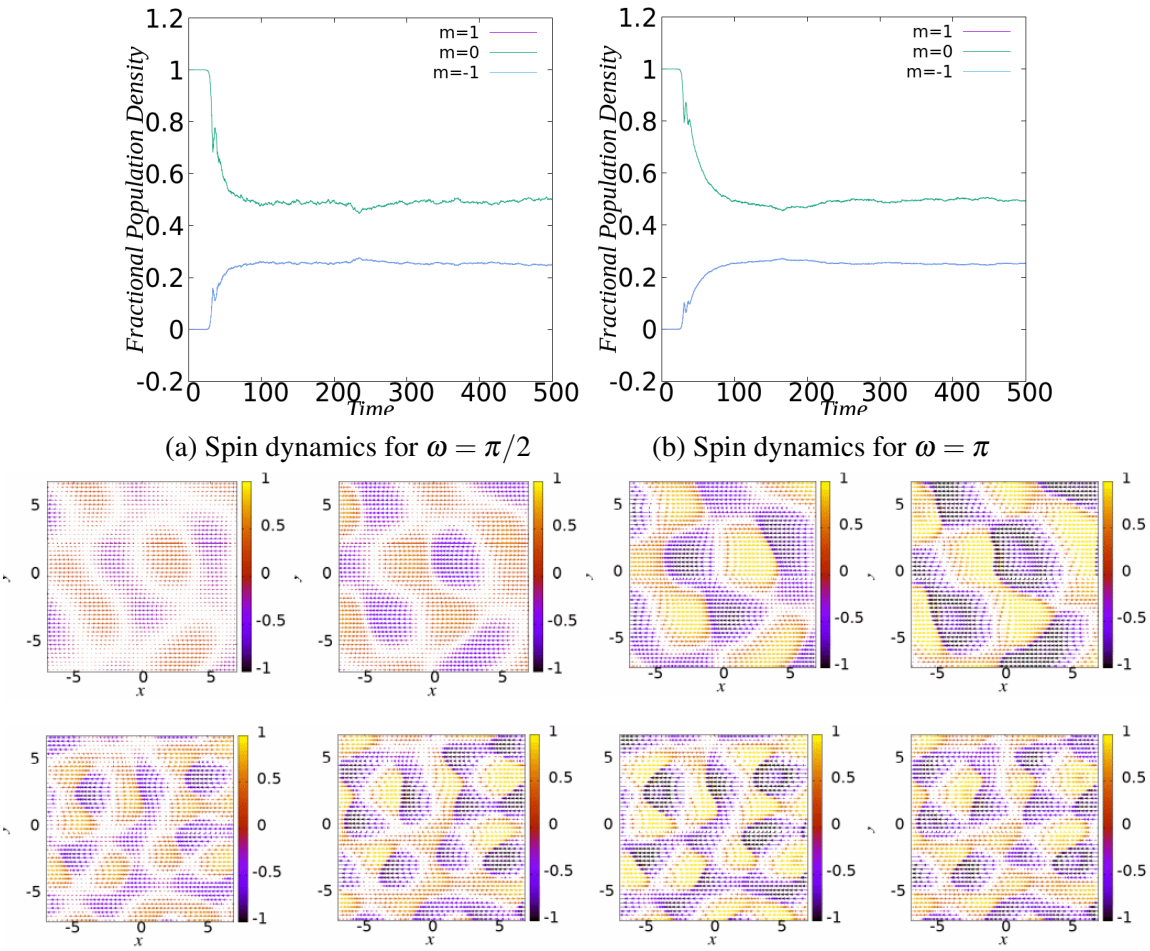

(a) Spin dynamics for $\omega = \pi/2$

(b) Spin dynamics for $\omega = \pi$

(c) Spin-textures in real space with time

Fig. 3.6 We observe flipping of directions of the spins in the spin-domains with time for both driving frequencies.

This spin dynamics shown in Figure [3.6] results in excitation of several k in the range $-2k_{\pm} < k_3, k_4 < 2k_{\pm}$ in the $m = 0$ component. The excitation of several k results in the pattern formed in the modulated system not having a definite symmetry.

We observe distinct patterns in the spin-textures-Figures[3.5]. The patterns are formed by spin-domains which appear to flip direction with time. The wavenumber of the patterns increases on increasing the modulation frequency. The wavenumber of these patterns offers us an important insight into elementary excitations of spinor BEC. In case the polar phase with a_0 scattering channel alone being modulated we observe patterns with wavenumber indicative of the resonant spin mode.

Spin-1 BEC with ferromagnetic interactions

We make similar observations when the interactions between spins is ferromagnetic as made when the interactions between the spins in the system is antiferromagnetic. The patterns in real space do not show any recognizable symmetry shown in Figure [3.7].This is again due to spin-dynamics (Figure [3.9]) that exchanges populations between the unstable excited spin mode (corresponding to population in the $m = \pm 1$ components) and the density mode (corresponding to population in the $m = 0$ component).

However,the wavenumber of the patterns increases on increasing the modulation frequency -Figures [3.7],[3.8]. The wavenumber of the pattern indicate the Bogoliubov mode resonant with the half the driving frequency. In this case it is the spin mode. The spin-textures form patterns with wavenumber corresponding to the second spin mode.

3.1.4 Spin-1 BEC in BA Phase

Homogeneous spinor field for the BA phase in the absence of any perturbation is given as:

$$\left(e^{i(\chi_0+\chi_z)} \frac{p\sqrt{f_z}(q+p)}{2}, e^{i\chi_0} \sqrt{\frac{(q^2-p^2)(-p^2-q^2+2c_1nq)}{4c_1nq^3}}, e^{i(\chi_0+\chi_z)} \frac{p\sqrt{f_z}(q-p)}{2} \right) e^{-i\mu t} \tag{3.24}$$

Here,$\mu = \frac{(-p^2+q^2+2qc_1n)^2}{8c_1nq^2} + \frac{c_0n}{2}$ and $f_z = \frac{p(-p^2+q^2+2qc_1n)}{2c_1nq^2}$

It is difficult to carry out linear stability analysis for this phase. However, we analyse the system numerically.

Spin-1 BEC with ferromagnetic interactions

We observe stripe like patterns in density space Figure-[3.10] of this phase on modulation with $\omega = \frac{\pi}{2}$ and square like patterns on modulation with $\omega = \pi$. The spin modes in the

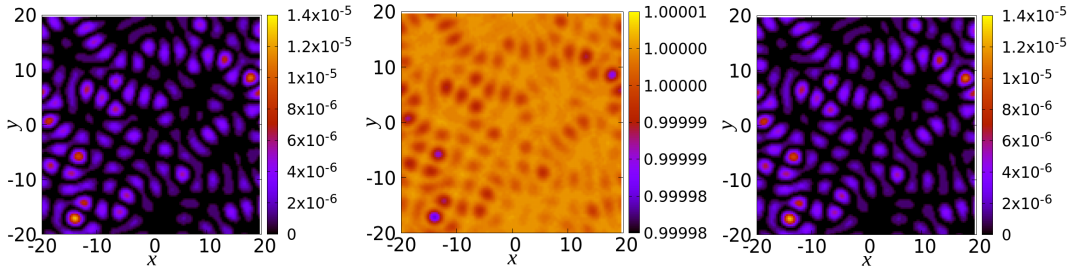

(a) m=1 component (b) m=0 component (c) m=-1 component

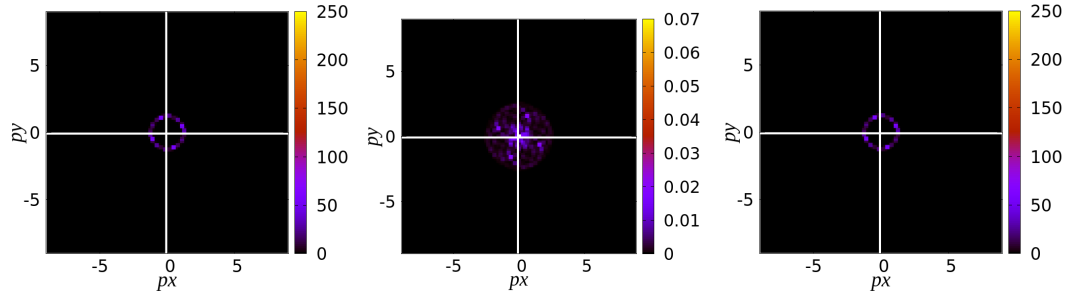

(d) m=1 component (e) m=0 component (f) m=-1 component

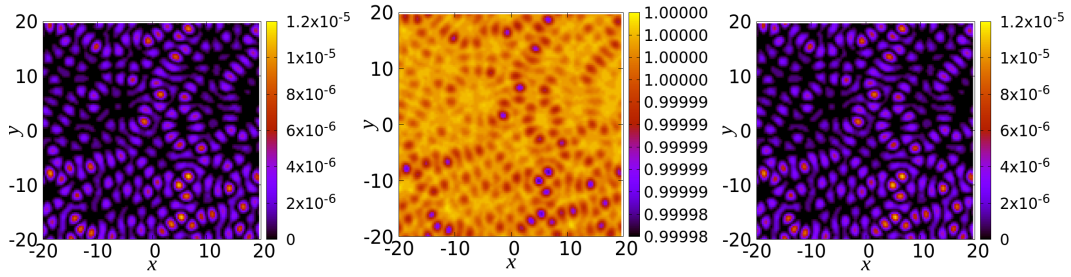

(g) m=1 component (h) m=0 component (i) m=-1 component

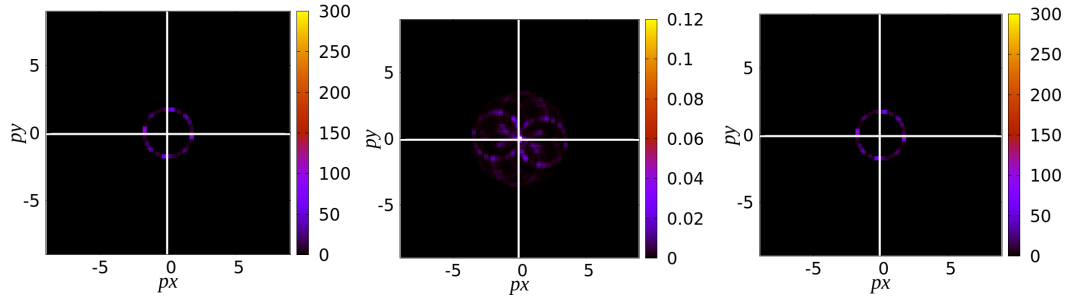

(j) m=1 component (k) m=0 component (l) m=-1 component

Fig. 3.7 Real and momentum space distribution of the different components of the Polar Phase spin-1 BEC with ferromagnetic interactions on periodic modulation of a_0 scattering channel with amplitude $\alpha = 0.2$ and for frequencies $\omega = \pi/2$ (above) and $\omega = \pi$ (below). The system shows patterns whose wavenumber increases (size decreases) with increasing modulation frequency. Here, the wavenumber of $m = \pm 1$ components corresponding to the unstable mode is $k = 1.25$ and $k = 1.79$ which compares well with the expected $k = 1.223$ and $k = 1.749$. The values of wavenumbers excited in the density mode are in the range of $-2k_{\pm} < k_0 < 2k_{\pm}$.

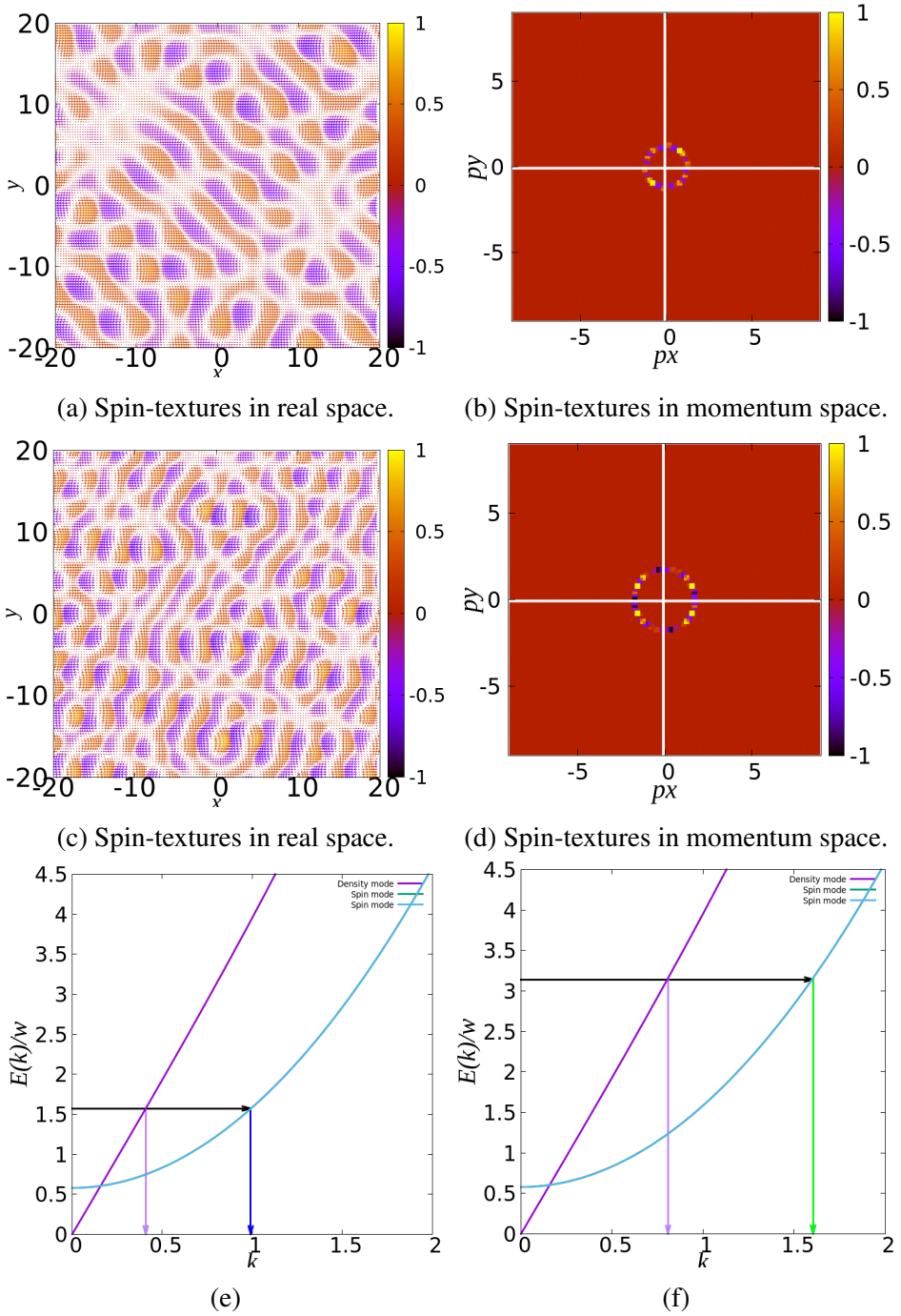

Fig. 3.8 Distribution of spins in real and momentum space for the polar phase of spin-1 BEC with ferromagnetic interactions on periodic modulation of a_0 scattering channel with amplitude $\alpha = 0.2$ and for frequencies $\omega = \pi/2$ (above) and $\omega = \pi$ (below). Here, the wavenumber of patterns formed by spin-textures corresponding to one of the spin modes is $k = 1.29$ and $k = 1.78$ which compares well with the expected wavenumbers of the spin $k = 1.223$ and $k = 1.749$. Fig.(e,f) shows dispersion relations obtained on solving the Bogoliubov spectra corresponding to the AFM phase. The arrows correspond to the modulating frequency and the corresponding wavenumber.

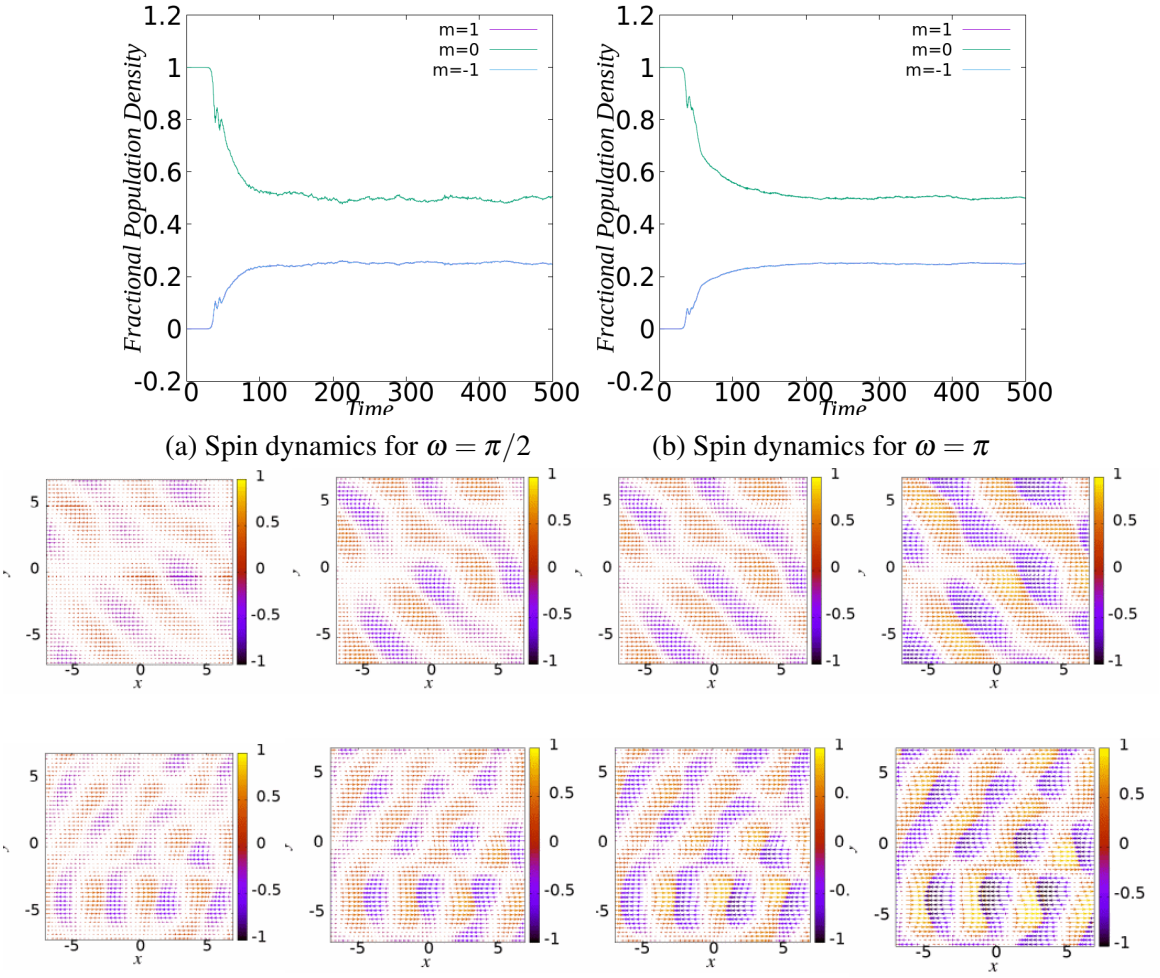

(a) Spin dynamics for $\omega = \pi/2$

(b) Spin dynamics for $\omega = \pi$

(c) Spin-textures in real space with time

Fig. 3.9 We observe flipping of directions of the spins in the spin-domains with time for both driving frequencies.

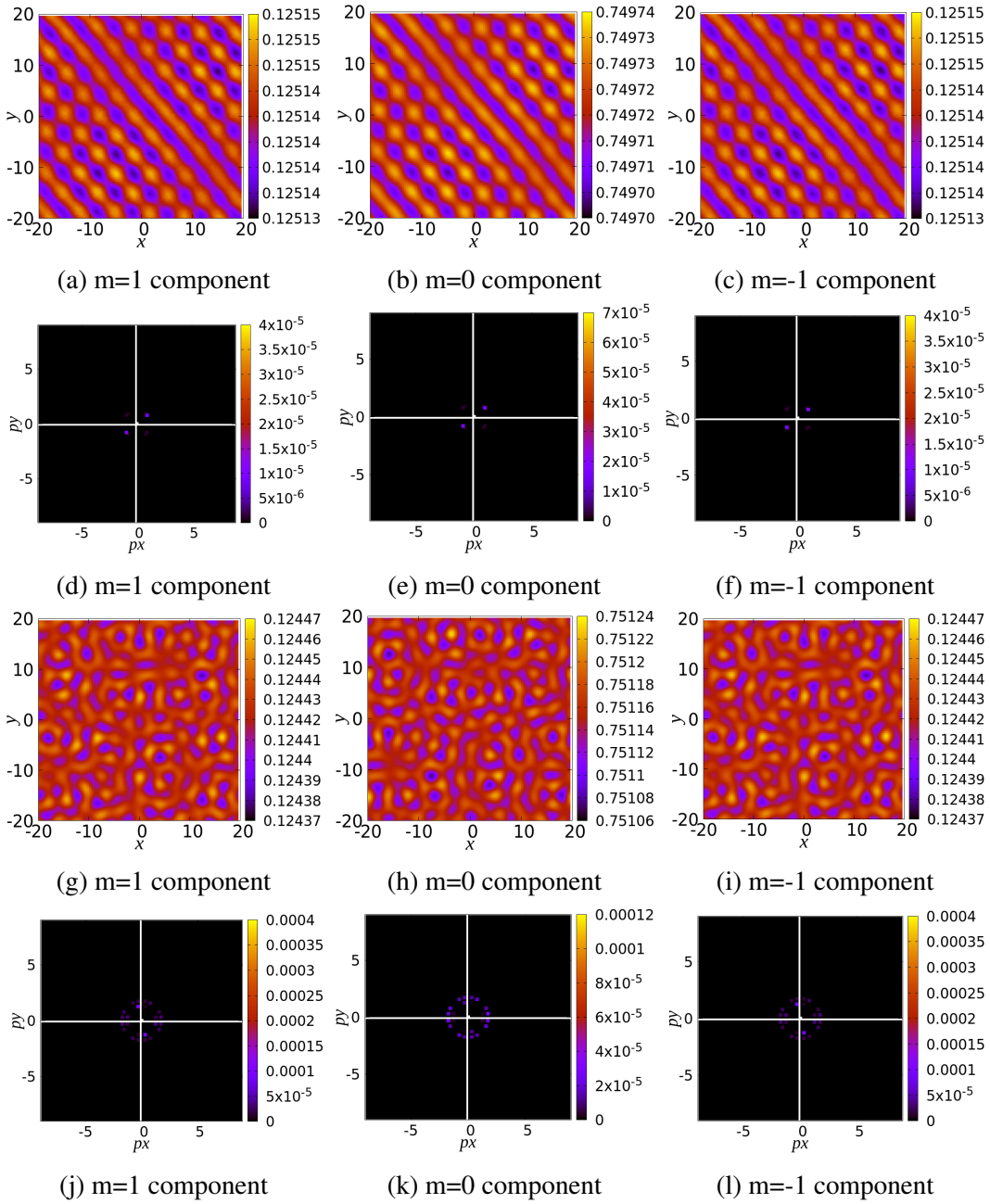

Fig. 3.10 Real and momentum space distribution of the different components of the BA phase spin-1 BEC on periodic modulation of a_0 scattering channel with amplitude $\alpha = 0.2$ and for frequencies $\omega = \pi/2$ (above) and $\omega = \pi$ (below). The system shows patterns whose wavenumber increases with increasing modulation frequency. Here, the wavenumber of $m = \pm 1$ components corresponding to the unstable spin mode is $k = 1.22$ and $k = 1.75$ which compares well with the expected $k = 1.25$ and $k = 1.766$.

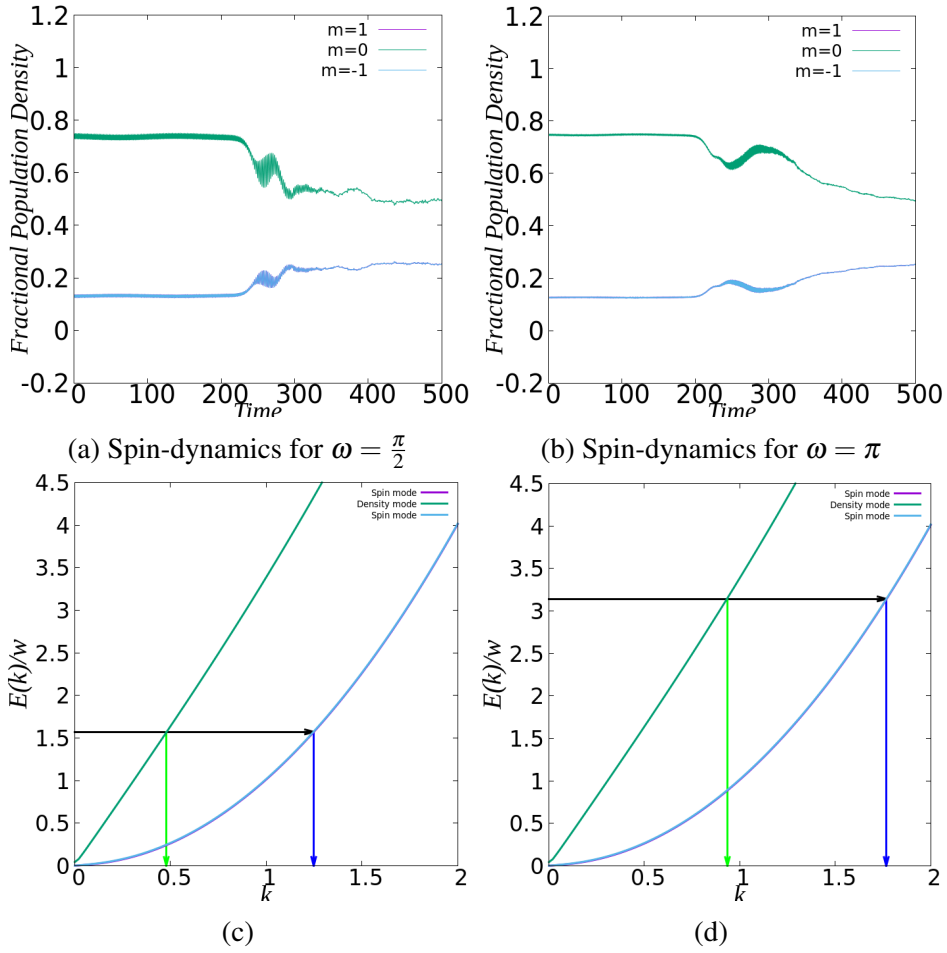

(a) Spin-dynamics for $\omega = \frac{\pi}{2}$ (b) Spin-dynamics for $\omega = \pi$

(c) (d)

Fig. 3.11 Spin-dynamics and dispersion relation of the BA phase with the arrows pointing the most unstable k corresponding to the modulation frequency.

BA phase couples all the components of the spin-1 BEC resulting in patterns in all three components. This complex coupling makes this phase difficult to analyse. We do not observe any spin dynamics (Figure-[3.11]) in the system when the system is stable (i.e, not heated as a results of the modulation). Thus we see patterns of definite symmetry as a single wavenumner-k is excited.

3.2 Summary

- Periodic modulation of the a_0 scattering channel leads to the excitation of spin modes in spin-1 BEC. The exception is ferromagnetic phase for which we see no excitation.
- The excitation of spin modes in the AFM and Polar phase is accompanied with spin dynamics, complex pattern and spin textures formation.
- In the BA phase we observe no spin dynamics and the pattern formation is much simpler with a single wavenumber being excited.
- We do not see patterns indicative of the density mode even though it has parametric instability because the parametric instability associated with the spin mode grows faster.

Chapter 4

Results and Discussions-II

4.1 Periodic modulation of the a_2 scattering channel

The $F = 2$ scattering channel is modulated with amplitude α and frequency ω. The $F = 0$ scattering channel is left time independent.

$$\tilde{a_2} = \tilde{a_2} + \tilde{a_2}(2\alpha\cos(2\omega t)) \tag{4.1}$$

The spin dependent and the spin independent interactions can then be written as

$$\tilde{c_0} = c_0 + 2\tilde{a_2}(2\alpha\cos(2\omega t)) \tag{4.2}$$

$$\tilde{c_1} = c_1 + \tilde{a_2}(2\alpha\cos(2\omega t)) \tag{4.3}$$

Here, $c_0 = \frac{4\pi(a_0+2a_2)\hbar^2}{3M}$ is the magnitude of the spin independent interaction between the atoms and $c_1 = \frac{4\pi(a_2-a_0)\hbar^2}{3M}$ is the strength of the spin-spin interaction between the atoms and $\tilde{a_2} = \frac{4\pi a_2\hbar^2}{3M}$. The modulation results in a spatially homogenous temporally modulated solution.

$$\Psi e^{[-i\mu t + \frac{\alpha a_2}{\omega}\sin(2\omega t)]} \tag{4.4}$$

Here, $\Psi = (\psi_+, \psi_0, \psi_-)$ is the spatially homogenous order parameter . A dynamical instability may arise in this system as a result of this modulation. We perform a linear stability analysis of this uniform state against a spatially and temporally modulated state.

$$(\Psi + \mathbf{w}\cos(\vec{k}.\vec{r}))e^{[-i\mu t + \frac{\alpha a_2}{\omega}\sin(2\omega t)]} \tag{4.5}$$

Here, $\mathbf{w} = (w_+, w_0, w_-)$ is is the complex-valued amplitude of the perturbation. Linear stability analysis is performed to determine if there might occur a spontaneous spatial

symmetry breaking as a result of modulation. We look at pattern formation in spin-1 BEC in the flat potenial limit. The methods and analysis remains similar to the previous section which looked at a_0 modulation. However, the patterns and dynamics of the different ground state phases changes as a different s-wave scattering channel is being modulated.

4.1.1 Spin-1 BEC in Ferromagnetic Phase

Homogeneous spinor field for the ferromagnetic phase in the absence of any perturbation is given as:

$$(1,0,0)e^{-i\mu t} \tag{4.6}$$

Here, $\mu = -p+q+c_0+c_1$. In the previous section we had observed no patterns in this phase as there was no two body scattering interaction with total spin $F=0$. However, we do expect pattern formation on perturbation of the a_2 scattering channel because all the two body interactions in this phase have total spin $F=2$. We proceed similar to the procedure outlined before. We first consider the spatially homogeneous system and find the spatially homogeneous and temporally modulated solution. We then perform linear stability analysis which compares the stability of uniform state against a spatial modulated state. The equations stated below gives the equation for real amplitude of the the spatial perturbation.

$$\frac{d^2u_+}{dt^2} + [k^2(k^2+2c_0+2c_1+4k^2\alpha\cos(2\omega t)]u_+ = 0 \tag{4.7}$$

$$\frac{d^2u_0}{dt^2} + [(k^2+p-q)^2]u_0 = 0 \tag{4.8}$$

$$\frac{du_-}{dt} - [(k^2+2p-2c_1-2\tilde{a_2}(2\alpha\cos(2\omega t))]v_- = 0 \tag{4.9}$$

$$\frac{dv_-}{dt} + [(k^2+2p-2c_1-2\tilde{a_2}(2\alpha\cos(2\omega t))]u_- = 0 \tag{4.10}$$

The amplitude of spatial modulation of the $m=1$ component of the BEC is described by a Mathieu equation. The solution of this equation gives an instability which grows in time. Thus,the spatially uniform $m=1$ component becomes unstable on the modulation of a_2 scattering channel. The equation describing the $m=-1$ component which also has the two body interactions that have total spin $F=2$ is more difficult to decouple or interpret. However,since the population of this component is negligible and there exists no spin-exchange process which might transfer population to this state, we can ignore the dynamics of this component.

Spin-1 BEC with antiferromagnetic interactions

Unlike modulation of a_0 scattering channel, modulation of a_2 scattering channel results in spontaneous spatial symmetry breaking of this phase. The results of numerical simulations are listed below. The real space show patterns indicative of the Bogoliubov mode resonant with half the driving frequency show in Figure-[4.1]. In this case we find density mode is the Bogoliubov mode that is excited.

$$(0,1)+(0,1) \rightarrow (k,1)+(-k,1) \tag{4.11}$$

The wave number of the patterns increases on increasing the driving frequency (Figure-[4.2]) in agreement with the dispersion relation of this mode. We observe no spin dynamics or spin-textures due to no spin-exchange collision and negligible populations in these spin modes.

Spin-1 BEC with ferromagnetic interactions

We make similar observations when the interactions between spins in ferromagnetic in nature. We observe square like patterns in real space (Figure-[4.3]) whose wavenumber increases on increasing the driving frequency in good agreement with the dispersion relation of the density mode (Figure-[4.4]). We also observe no spin-dynamics or spin-textures.

4.1.2 Spin-1 BEC in Antierromagnetic Phase

Homogeneous spinor field for the antiferromagnetic phase in the absence of any perturbation is given below:

$$\left(\sqrt{\frac{1+\frac{p}{c_1}}{2}}, 0, \sqrt{\frac{1-\frac{p}{c_1}}{2}}\right) e^{-i\mu t} \tag{4.12}$$

Here,$\mu = q + c_0 n$. This phase is present only when the interactions between spins is anti-ferromagnetic in nature. To simplify our calculations we take $p = 0$. We find the uniform solutions of the system on temporal modulation and then perform linear stability analysis to check its stability against spatially modulated states and obtain the following equations for

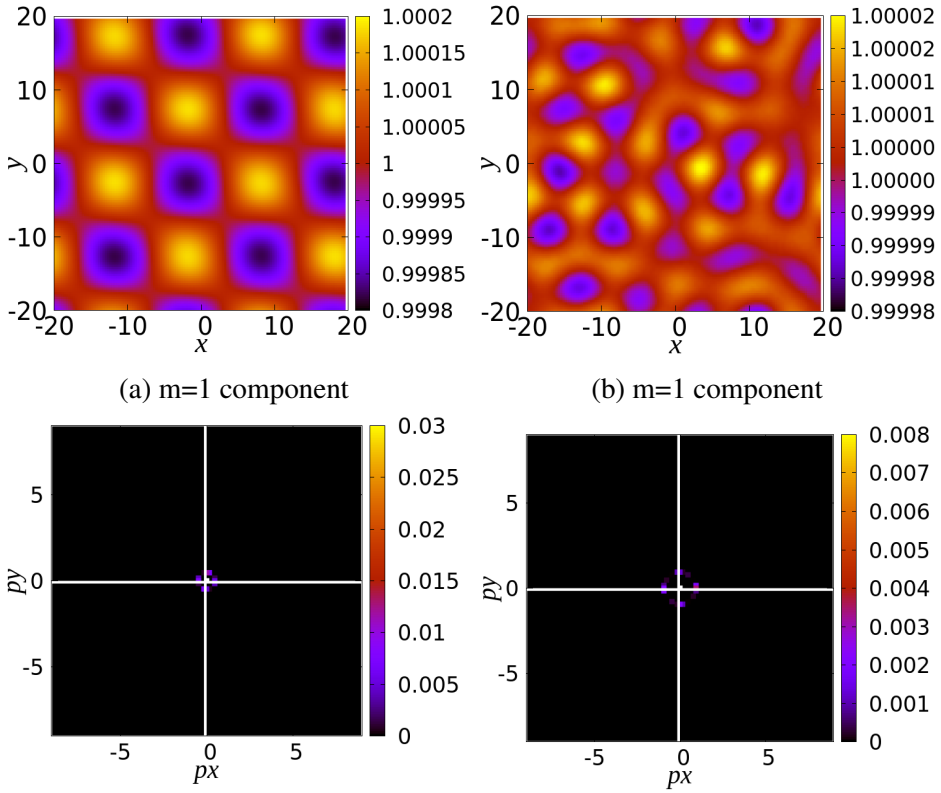

(a) m=1 component (b) m=1 component

(c) m=1 component (d) m=1 component

Fig. 4.1 Real and momentum space distribution of the spatially modulated component of the FM phase spin-1 BEC with antiferromagnetic interactions on periodic modulation of a_2 scattering channel with amplitude $\alpha = 0.2$ and for frequencies $\omega = \pi/2$ (above) and $\omega = \pi$ (below). The system shows patterns whose wavenumber increases with increasing modulation frequency. Here, the wavenumber of the components corresponding to the unstable mode is $k = 0.48$ and $k = 0.93$ which compares well with the expected $k = 0.45$ and $k = 0.90$.

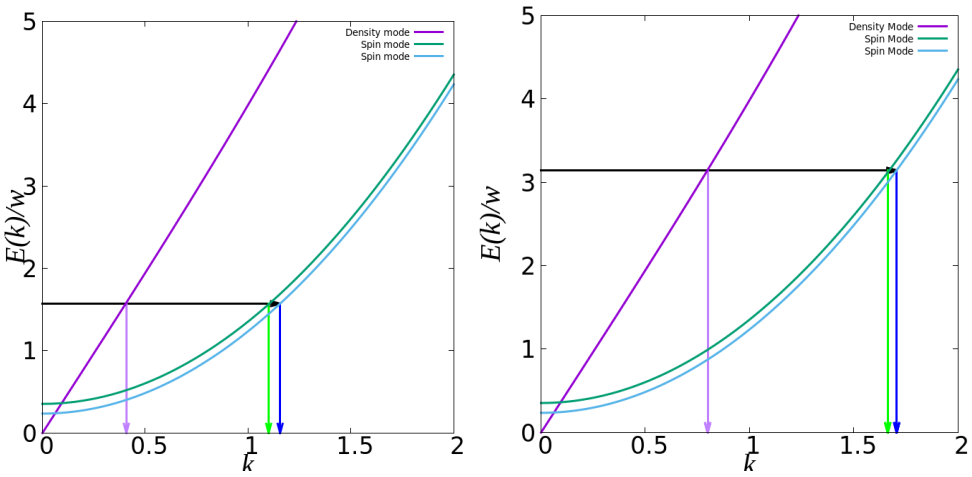

(a) (b)

Fig. 4.2 Dispersion relation of the modes of FM phase with antiferromagnetic interactions.

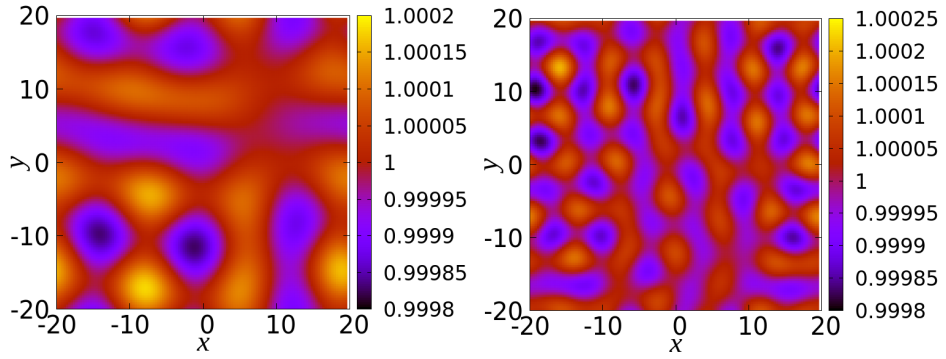

(a) m=1 component (b) m=1 component

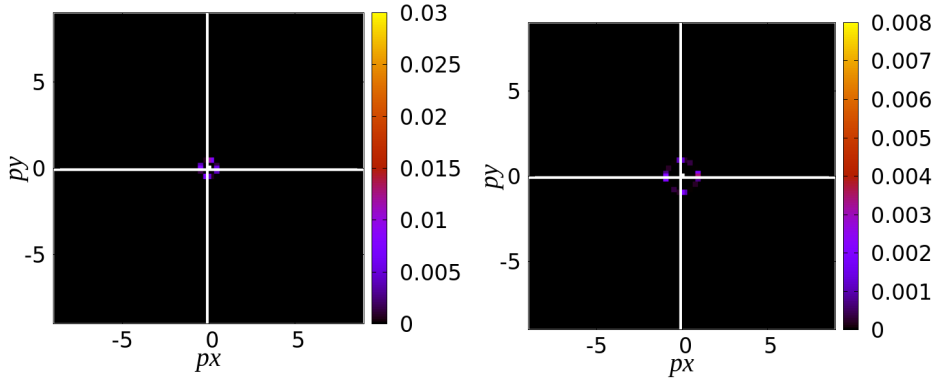

(c) m=1 component (d) m=1 component

Fig. 4.3 Real and momentum space distribution of the spatially modulated components of the FM phase spin-1 BEC with ferromagnetic interactions on periodic modulation of a_2 scattering channel with amplitude $\alpha = 0.2$ and for frequencies $\omega = \pi/2$ (above) and $\omega = \pi$ (below). Here, the wavenumber of the components corresponding to the unstable density mode is $k = 0.501$ and $k = 0.93$ which compares well with the expected $k = 0.48$ and $k = 0.93$.

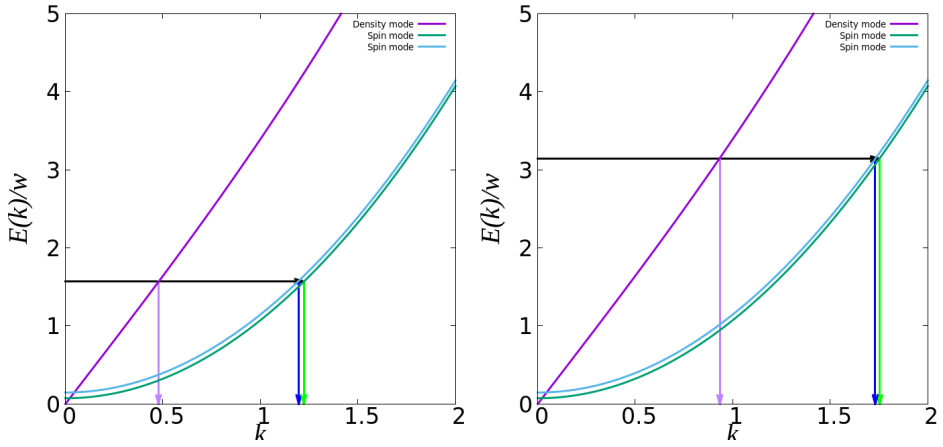

(a) (b)

Fig. 4.4 Dispersion relation of the modes of FM phase with ferromagnetic interactions.

the real amplitude of spatial modulation.

$$\frac{\partial^2\zeta_+}{\partial t^2}+[(k^2+2c_0)k^2+k^2(4\tilde{a_2})(2\alpha\cos(2\omega t))]\zeta_+ = 0 \quad (4.13)$$

$$\frac{\partial^2\zeta_-}{\partial t^2}+[(k^2+2c_1)k^2+k^2(2\tilde{a_2})(2\alpha\cos(2\omega t))]\zeta_- = 0 \quad (4.14)$$

$$\frac{\partial^2 u_0}{\partial t^2}+[(k^2-q+2c_1)(k^2-q)+(k^2-q)(2\tilde{a_2})(2\alpha\cos(2\omega t))]u_0 = 0 \quad (4.15)$$

Solution to these equations is obtained using the Floquet theorem. The Floquet exponent $\sigma_m = \sigma_m(\omega,\alpha,k)$ determines the stability of these solutions.The system is unstable if $Re(\sigma_m) > 0$. On solving the two Mathieu equations we make the following observations:

- Both the density and spin modes are rendered unstable on periodic driving of the a_2 scattering channel.
- $\sigma_0 > \sigma_\pm$
  - For $\omega = \frac{\pi}{2}$, the floquet exponent corresponding to most unstable k of each mode are compared i.e, the floquet exponent corresponding to most unstable k of each mode are compared i.e, the floquet exponent corresponding to most unstable k of each mode are compared i.e, the floquet exponent corresponding to most unstable k of each mode are compared i.e, $\sigma_+ = 0.0625668$-density mode,$\sigma_- = 0.495733$-spin mode $< \sigma_0 = 0.495734$-spin mode.

  - For $\omega = \pi$, the floquet exponent corresponding to most unstable k of each mode are compared i.e,$\sigma_+ = 0.060545$-density mode,$\sigma_- = 0.273984$-spin mode $< \sigma_0 = 0.273986$-spin mode.

- This implies that the spin mode is the most unstable and will grow faster than the others.

We expect to see spin-dynamics as population transfers from the density mode to the spin mode via the spin-exchange process:

$$(0,1)+(0,-1) \rightarrow (k,0)+(-k,0) \tag{4.16}$$

The observations in terms of which mode is made unstable remains same as when a_0 scattering channel is modulated.

The real and momentum space distribution is given in Figures- [4.5], [4.6] ,spin-textures and spin dynamics are shown in the Figure [4.7].

$$(k_1,0)+(k_2,0) \rightarrow (k_3,1)+(k_4,-1) \tag{4.17}$$

$$|k_1| = |k_2| = k \tag{4.18}$$

The patterns in real space do not show have any discernible symmetry due to the multiple modes in the range of $-2k < (k_3,k_4) < 2k$ being unstable at the same time as a result of dynamics described above.

The patterns formed by the spin-textures on the other hand show more distinct patterns indicative of the spin mode corresponding to $m = \pm 11$ spin mode. The patterns are formed by spin-domains which appear to flip direction with time.

The wavenumber of the patterns increases on increasing the modulation frequency. We observe patterns with wavenumber indicative of the resonant spin mode. Even though the mode selected is same as the one selected when a_0 scattering channel was modulated, the symmetry in the spin-textures is much different when a_2 scattering channel is modulated.

4.1.3 Spin-1 BEC in Polar Phase

Homogeneous spinor field for the polar phase in the absence of any perturbation is given as:

$$(0,1,0)e^{-i\mu t} \tag{4.19}$$

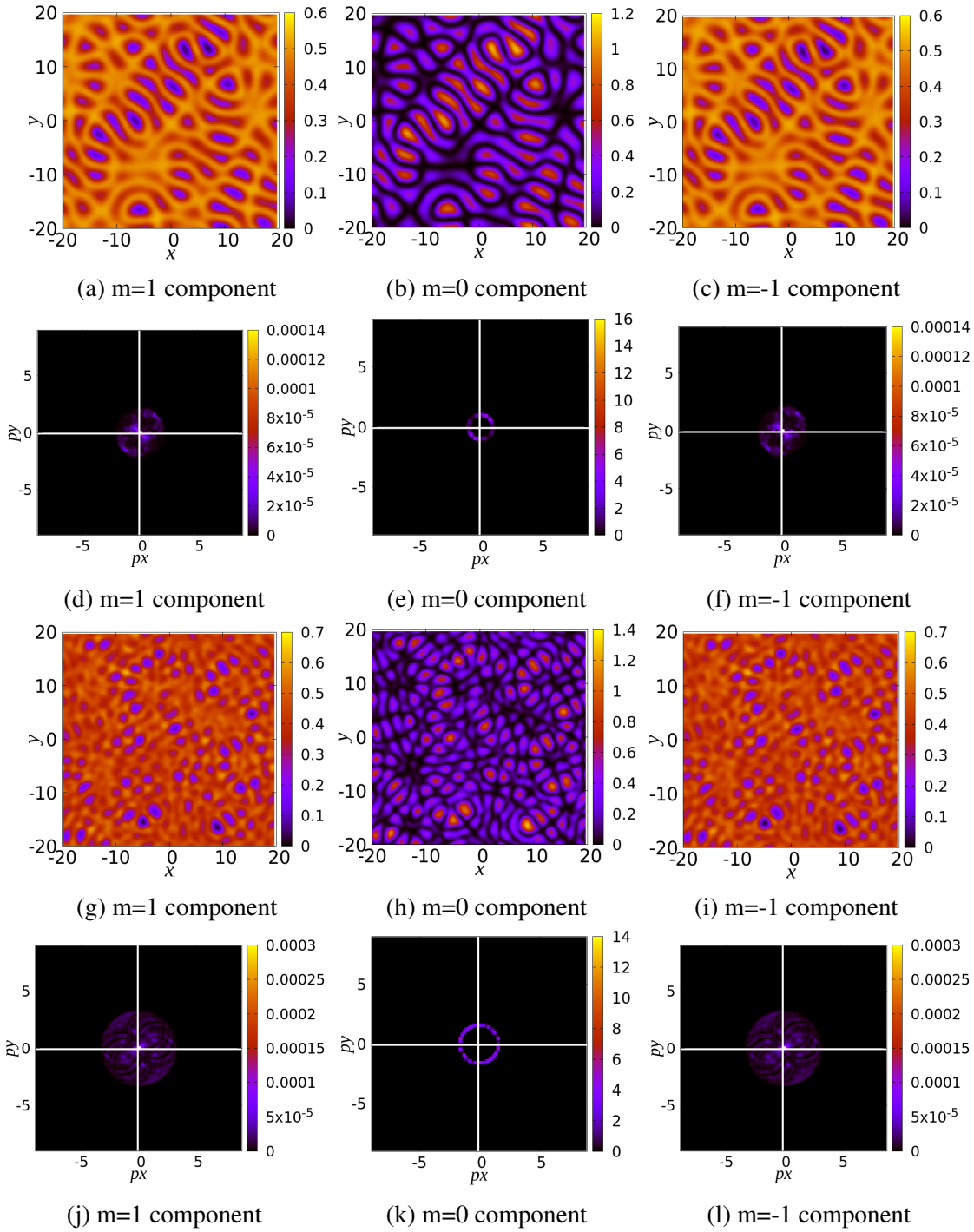

Fig. 4.5 Real and momentum space distribution of the different components of the AFM phase spin-1 BEC on periodic modulation of a_2 scattering channel with amplitude $\alpha = 0.2$ and for frequencies $\omega = \pi/2$ (above) and $\omega = \pi$ (below). Here, the wavenumber of $m = 0$ component corresponding to the unstable mode is $k_0 = 1.01$ and $k_0 = 1.56$ which compares well with the expected $k_0 = 0.993$ and $k = 1.598$. The values of wavenumbers excited in the other components are in the range of $-2k_0 < k_\pm < 2k_0$..

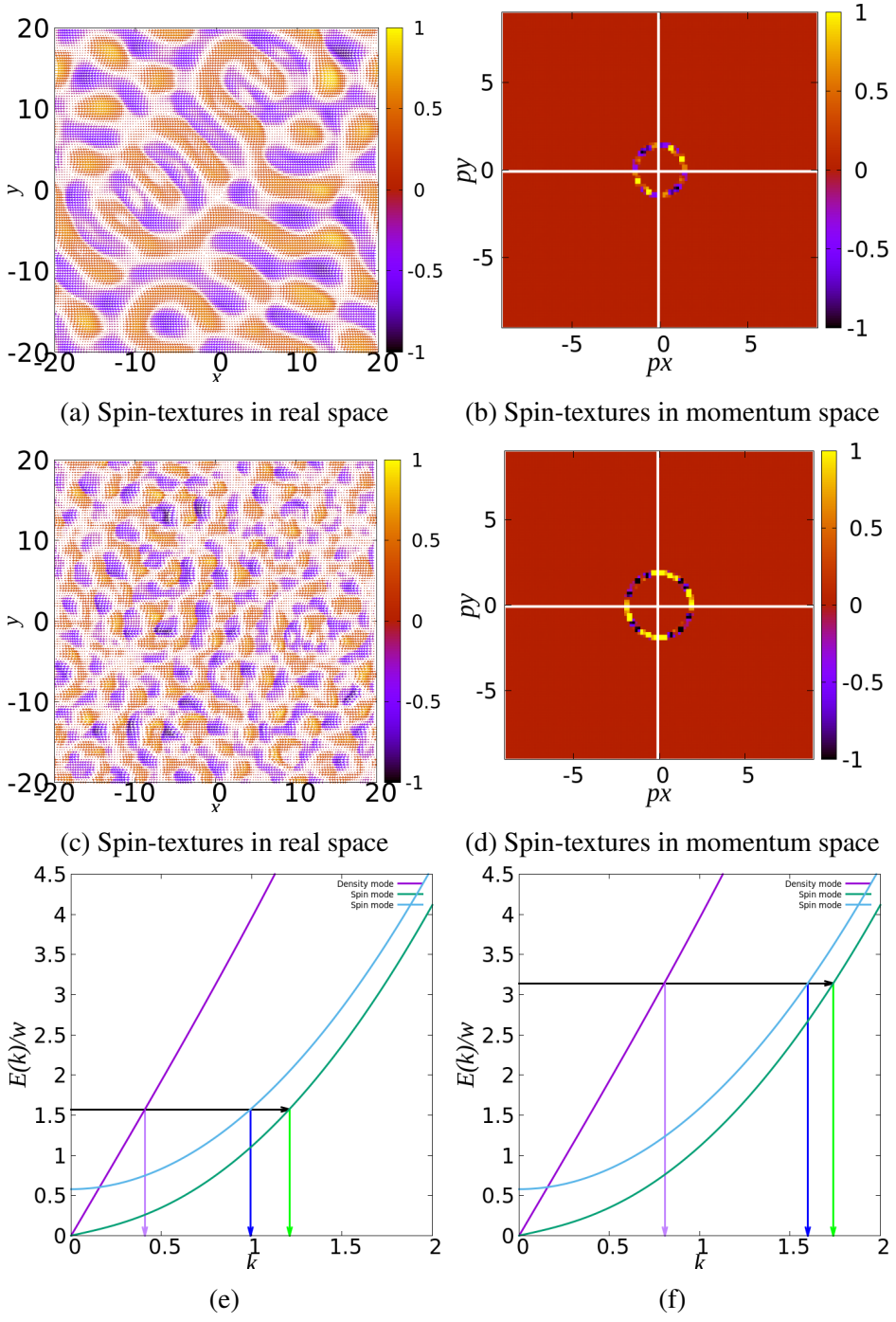

(a) Spin-textures in real space (b) Spin-textures in momentum space

(c) Spin-textures in real space (d) Spin-textures in momentum space

(e) (f)

Fig. 4.6 Distribution of spins in real space for the AF phase of spin-1 BEC with antiferromagnetic interactions on periodic modulation of a_2 scattering channel with amplitude $\alpha = 0.2$ and for frequencies $\omega = \pi/2$(above) and $\omega = \pi$ (below). Here, the wavenumber of pattens formed by spin-textures corresponding to one of the spin modes is $k = 1.40$ and $k = 1.67$ which compares well with the expected wavenumbers of the density mode $k = 1.209$ and $k = 1.739$. Fig.(e,f) shows dispersion relations obtained on solving the Bogoliubov spectra corresponding to the AF phase. The arrows correspond to the modulating frequency and the corresponding wavenumber.

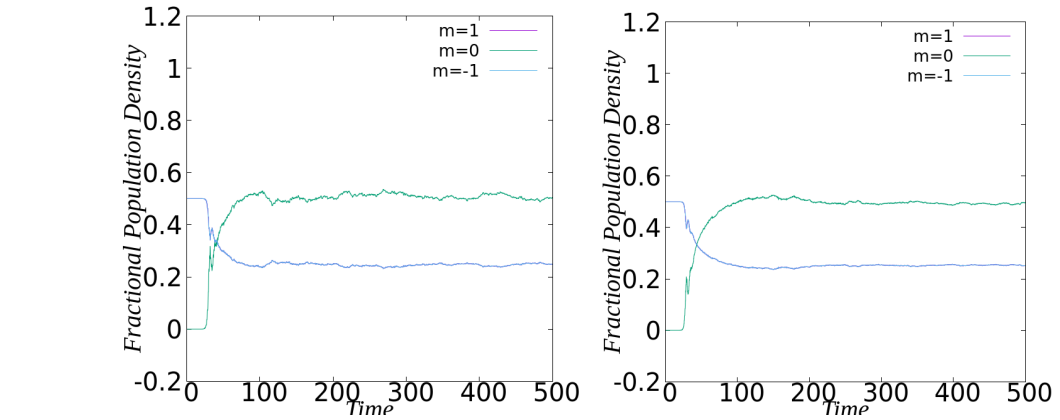

(a) Spin dynamics for $\omega = \pi/2$ (b) Spin dynamics for $\omega = \pi$

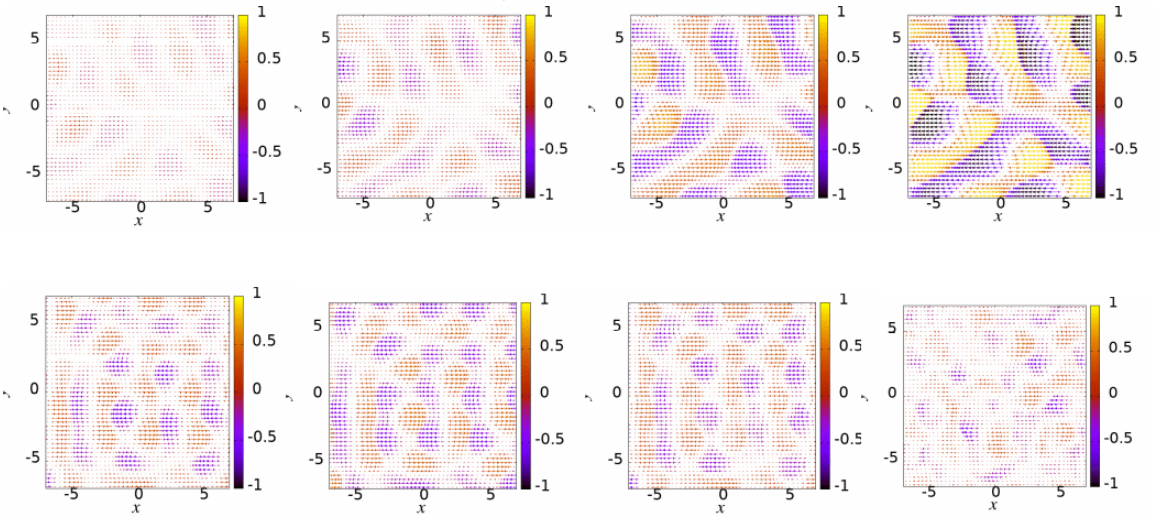

(c) Spin-textures in real space with time

Fig. 4.7 We observe flipping of spin-domains in time in the spin-textures in real space.

Here,$\mu = c_0$. We also consider $p = 0$ to simplify the calculations. We arrive at the equations describing the dynamics of the system by performing a linear stability analysis to test if the translational symmetry may be broken on perturbation.We arrive at the following equations for the real amplitude of spatial perturbations:

$$\frac{\partial^2 \zeta_+}{\partial t^2} - [-(k^2+q+c_1)(k^2+q) + (k^2+q)(2\tilde{a_2})(2\alpha\cos(2\omega t))]\zeta_+ = 0 \quad (4.20)$$

$$\frac{\partial^2 u_0}{\partial t^2} + [(k^2+2c_0)k^2 + k^2(4\tilde{a_2})(2\alpha\cos(2\omega t))]u_0 = 0 \quad (4.21)$$

Here, $\zeta_+ = u_+ + u_-$. The real amplitude of both the density mode and the coupled spin mode is described by Mathieu equations. The stability of this Mathieu equations is given by the real part of the floquet exponent of each mode. On solving the above equations we make the following observations:

- Both the density mode and coupled spin mode are rendered unstable on periodic driving of the a_2 scattering channel.
- $\sigma_0 < \sigma_\pm$
  - Antiferromagnetic interactions
    - For $\omega = \frac{\pi}{2}$, the floquet exponent corresponding to most unstable k of each mode are compared i.e, the floquet exponent corresponding to most unstable k of each mode are compared i.e, the floquet exponent corresponding to most unstable k of each mode are compared i.e, $\sigma_+ = 0.0625668$-density mode $< \sigma_0 = 0.495734$-spin mode.
    - For $\omega = \pi$, the floquet exponent corresponding to most unstable k of each mode are compared i.e,the floquet exponent corresponding to most unstable k of each mode are compared i.e,$\sigma_+ = 0.060545$-density mode $< \sigma_0 = 0.273986$-spin mode.
  - Ferromagnetic interactions
    - For $\omega = \frac{\pi}{2}$, the floquet exponent corresponding to most unstable k of each mode are compared i.e, the floquet exponent corresponding to most unstable k of each mode are compared i.e, the floquet exponent corresponding to most unstable k of each mode are compared i.e, $\sigma_+ = 0.0659502$-density mode $< \sigma_0 = 0.428482$-spin mode.
    - For $\omega = \pi$, the floquet exponent corresponding to most unstable k of each mode are compared i.e,$\sigma_+ = 0.0622128$-density mode $< \sigma_0 = 0.222552$-spin mode.

- From the floquet exponents the spin mode is the most unstable and will grow faster compared to the others.

When the system is in this phase, there exists two-body spin exchange process that conserves spin and can transfer population from the $m = 0$ components to the $m = \pm 1$ components.

$$(0,0) + (0,0) \rightarrow (k,1) + (-k,-1) \tag{4.22}$$

We expect translational symmetry breaking and spin-dynamics as population is transferred from the $m = \pm 1$ components corresponding to the density mode to the more unstable $m = 0$ component corresponding to the spin mode. We performed numerical simulations to study this system for both kinds of spin interactions.

Spin-1 BEC with antiferromagnetic interactions

The results of numerical simulation are shown in Figures [4.8, 4.9, 4.10] Patterns in real space do not show have any specific symmetry and are similar to the AF phase Figure-[4.8]. This is because of spin-dynamics which tries to restore the excited population in the component corresponding to spin mode back to the $m = 0$ component. This results in the several wavenumbers in the range of $-2k < (k_3, k_4) < 2k$ being excited and no specific symmetry in the patterns formed.

We observe distinct patterns in the spin-textures. The patterns are formed by spin-domains which appear to flip direction with time. Patterns formed by the spin domains when a_2 is modulated has a different symmetry when compared to patterns formed on modulation of a_0 scattering channel.

The wavenumber of these patterns offers us an important insight into elementary excitations of spinor BEC. In case the polar phase with a_2 scattering channel alone being modulated we observe patterns with wavenumber indicative of the resonant spin mode. The wavenumber of the patterns increases on increasing the modulation frequency in good agreement with the dispersion relation of the spin mode.

Spin-1 BEC with ferromagnetic interactions

We make similar observations when the interactions between the spins in the system is ferromagnetic shown in Figures- [4.11, 4.12]. The patterns in real space do not show any recognizable symmetry due to spin dynamics and several k being excited due to the processes explained in the previous chapter. The wavenumber of the pattern indicate the Bogoliubov mode resonant with the half the driving frequency. In this case it is the spin mode.

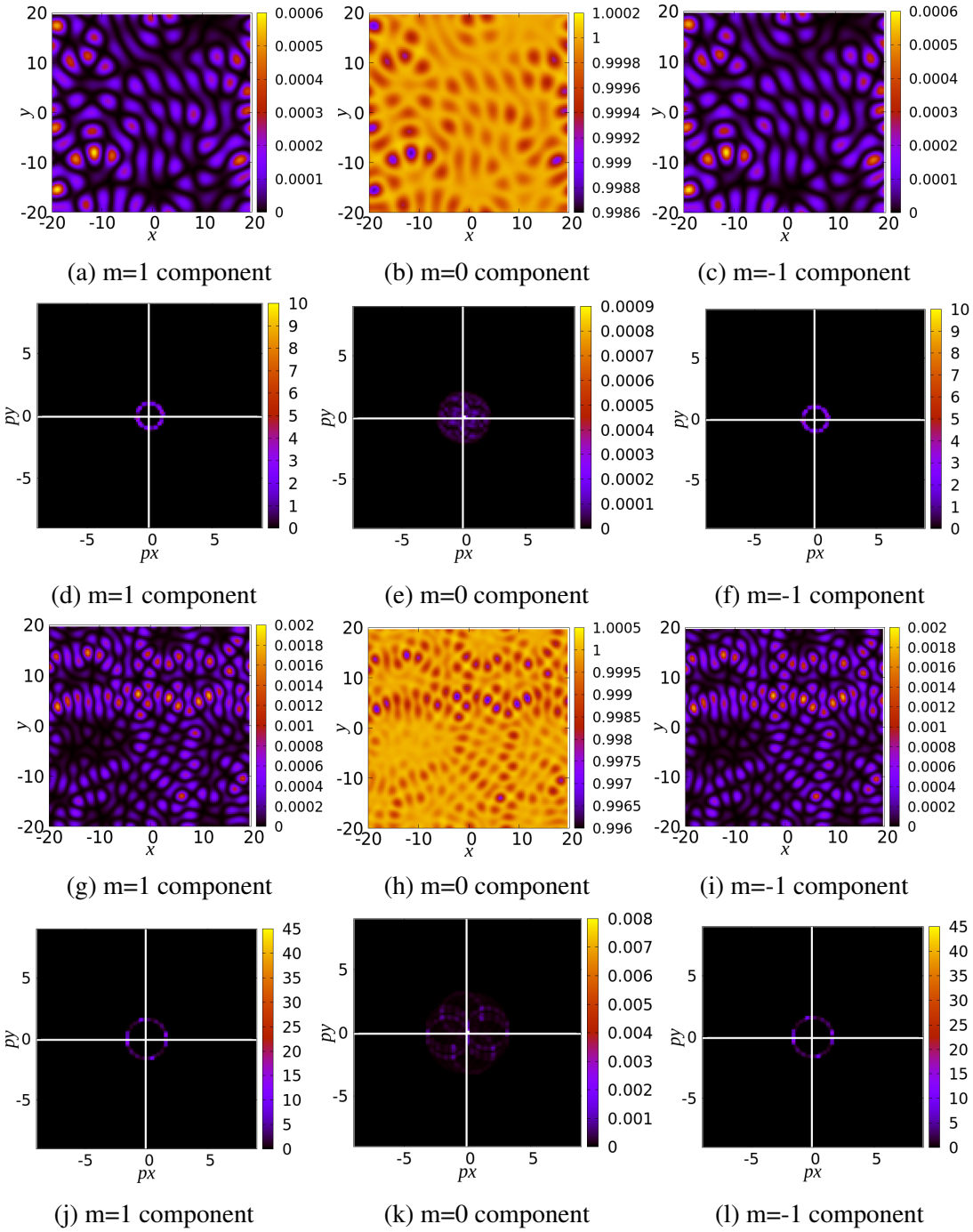

Fig. 4.8 Real space distribution of the different components of the Polar phase spin-1 BEC with antiferromagnetic interactions on periodic modulation of a_2 scattering channel with amplitude $\alpha = 0.2$ and for frequencies $\omega = \pi/2$ (above) and $\omega = \pi$ (below). The system shows patterns whose wavenumber increases with increasing modulation frequency. Here, the wavenumber of components corresponding to the unstable mode is $k_0 = 1.01$ and $k_0 = 1.62$ which compares well with the expected $k_0 = 0.991$ and $k = 1.6039$. The values of wavenumbers excited in the density mode are in the range of $-2k_0 < k_\pm < 2k_0$.

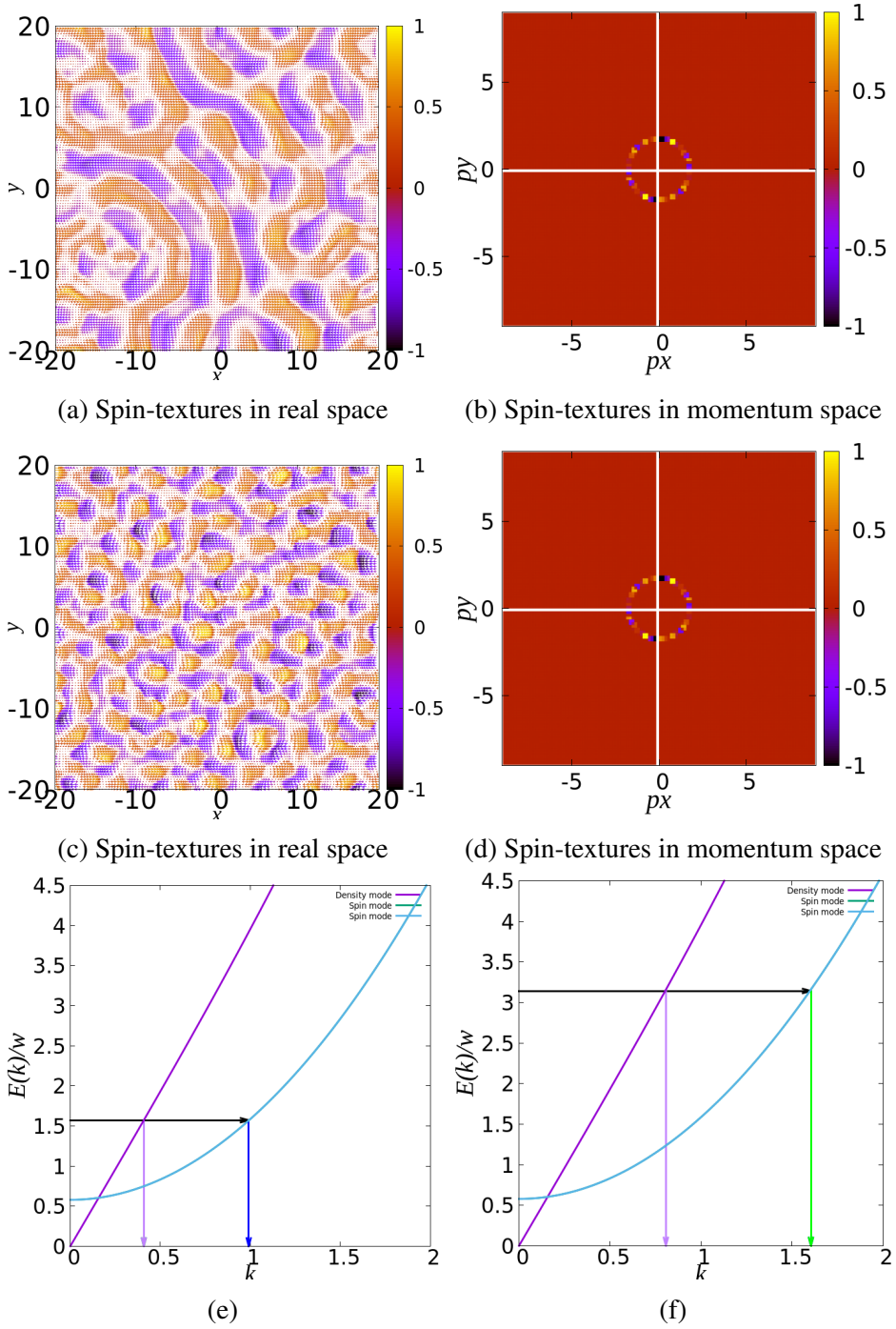

(a) Spin-textures in real space (b) Spin-textures in momentum space

(c) Spin-textures in real space (d) Spin-textures in momentum space

(e) (f)

Fig. 4.9 Distribution of spins in real and momentum space for the Polar phase of spin-1 BEC with antiferromagnetic interactions on periodic modulation of a_2 scattering channel with amplitude $\alpha = 0.2$ and for frequencies $\omega = \pi/2$ (above) and $\omega = \pi$ (below). Here, the wavenumber of patterns formed by spin-textures corresponding to one of the spin modes is $k = 1.01$ and $k = 1.63$ which compares well with the expected wavenumbers of the spin $k = 0.991$ and $k = 1.604$. Fig.(e,f) shows dispersion relations obtained on solving the Bogoliubov spectra corresponding to the Polar phase. The arrows correspond to the modulating frequency and the corresponding wavenumber.

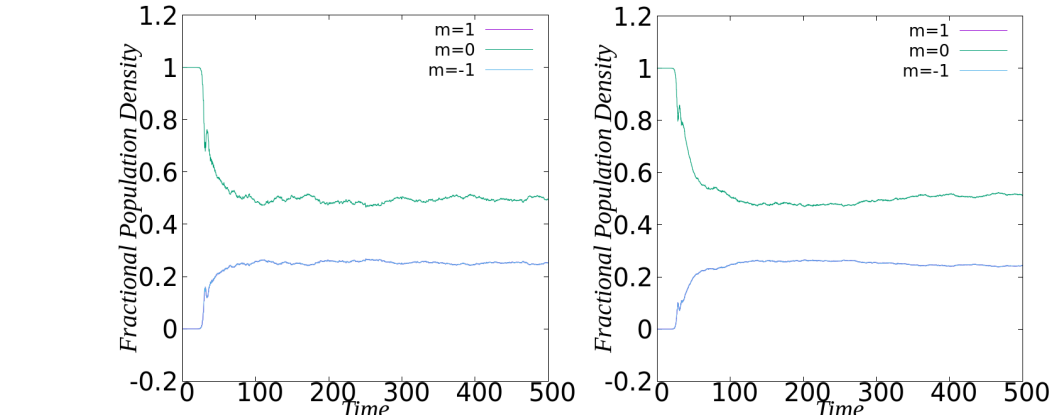

(a) Spin dynamics for $\omega = \pi/2$ (b) Spin dynamics for $\omega = \pi$

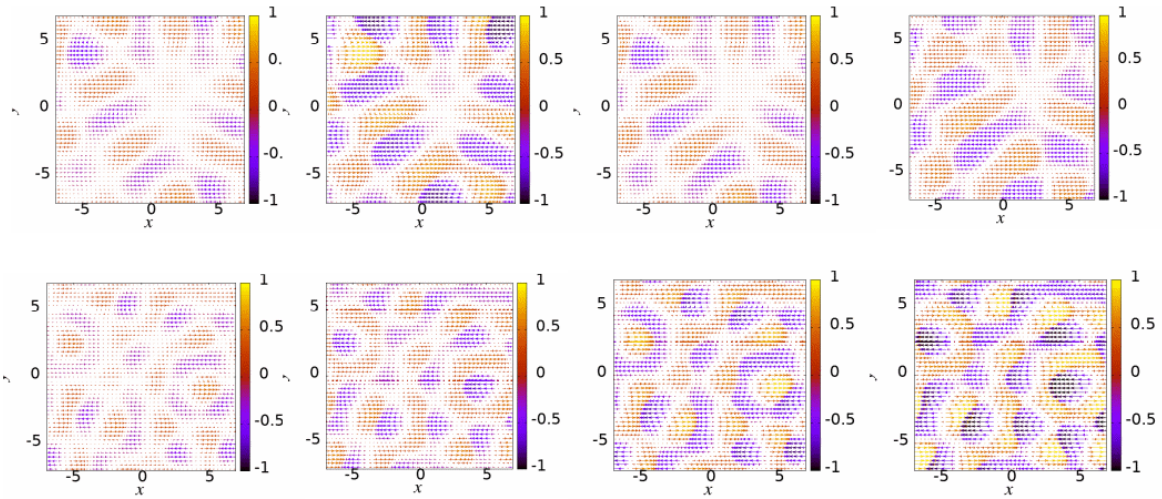

(c) Spin-textures in real space with time

Fig. 4.10 We observe flipping of spin-domains in time in the spin-textures in real space.

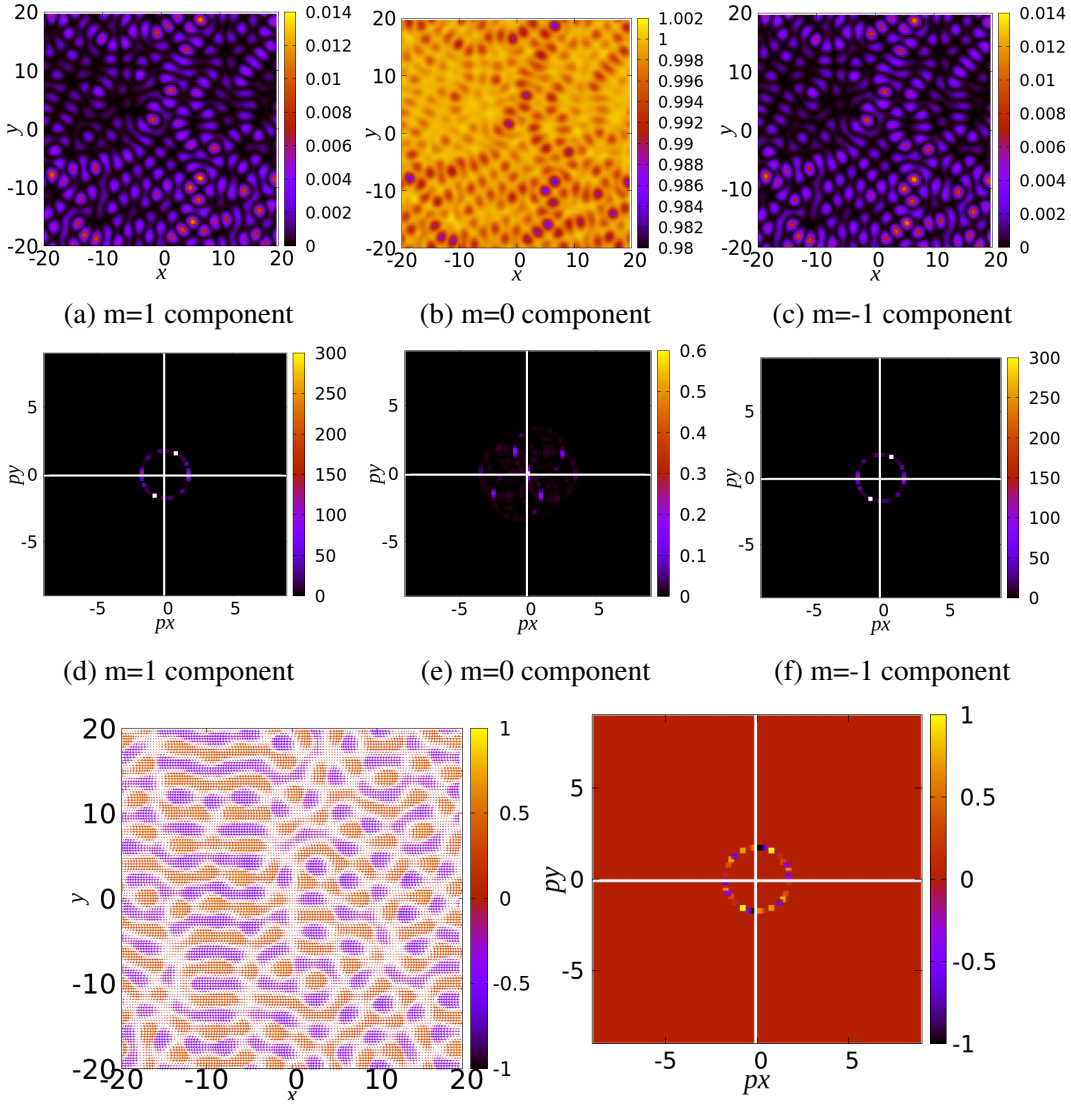

Fig. 4.11 Real and momentum space distribution of the different components of the Polar phase spin-1 BEC with ferromagnetic interactions on periodic modulation of a_2 scattering channel with amplitude $\alpha = 0.2$ and for frequency $\omega = \pi$. Here, the wavenumber of $m = \pm 1$ components corresponding to the unstable mode is $k = 1.77$ which compares well with the expected $k = 1.75$. The last two figures shows distribution of spins in real space and momentum space. Here, the wavenumber of patterns formed by spin-textures corresponding to one of the spin modes is $k = 1.85$ which compares well with the expected $k = 1.78$. The values of wavenumbers excited in the density mode are in the range of $-2k_0 < k_\pm < 2k_0$.

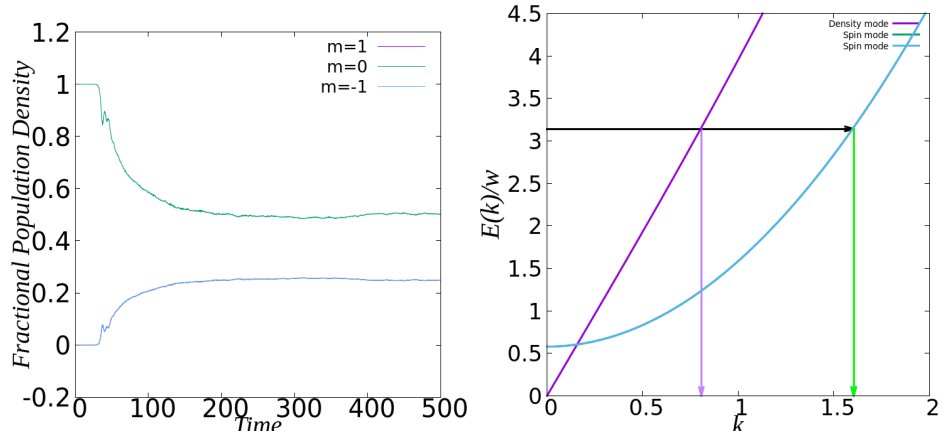

(a) (b)

Fig. 4.12 (a)Spin-dynamics on modulation of the a_2 scattering channel. (b)Dispersion relations obtained on solving the Bogoliubov spectra corresponding to the Polar phase. The arrows correspond to the modulating frequency and the corresponding wavenumber

4.1.4 Spin-1 BEC in BA Phase

Homogeneous spinor field for the BA phase in the absence of any perturbation is given as:

$$(e^{i(\chi_0+\chi_z)}\frac{p\sqrt{f_z}(q+p)}{2}, e^{i\chi_0}\sqrt{\frac{(q^2-p^2)(-p^2-q^2+2c_1nq)}{4c_1nq^3}}, e^{i(\chi_0+\chi_z)}\frac{p\sqrt{f_z}(q-p)}{2})e^{-i\mu t} \tag{4.23}$$

Here,$\mu = \frac{(-p^2+q^2+2qc_1n)^2}{8c_1nq^2} + \frac{c_0n}{2}$ and $f_z = \frac{p(-p^2+q^2+2qc_1n)}{2c_1nq^2}$.This phase is possible only in spin-1 BEC with ferromagnetic interactions between the spins.

It is difficult to analyse this phase for spontaneous translational symmetry breaking analytically. However, we study pattern formation in this system using numerical simulations.

Spin-1 BEC with ferromagnetic interactions

We observe square like patterns in density space of this phase on modulation with frequencies $\omega = \frac{\pi}{2}$ and $\omega = \pi$ (Figure- [4.13]). The symmetry and wave number of the patterns is different from when a_0 scattering channel was modulated.The wavenumber of the pattern is reflective of one of the spin modes (Figure- [4.14]). Again, we see no spin-textures in this phase as there is no spin-dynamics in the initial states when the system is stable and not heated.

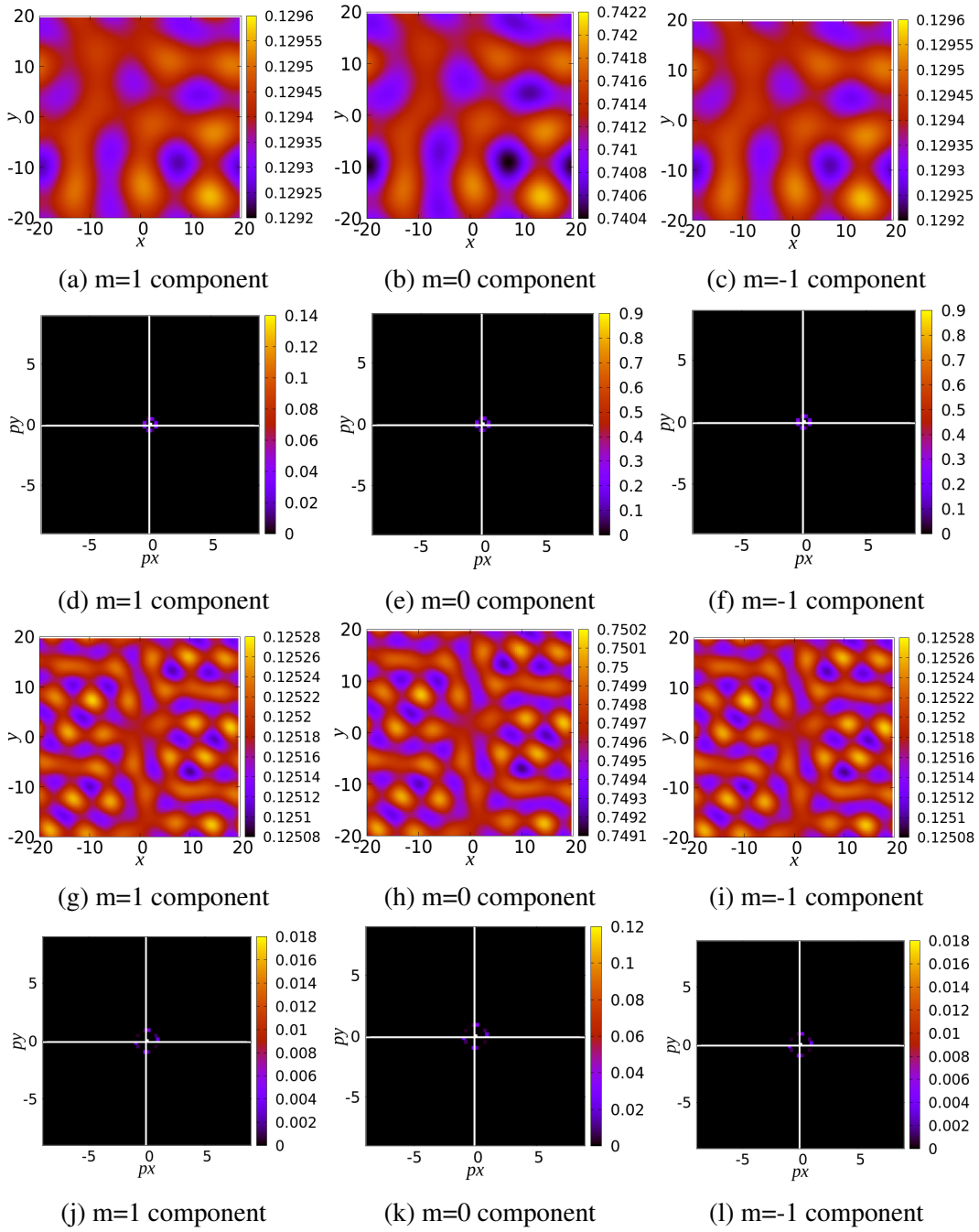

Fig. 4.13 Real and momentum space distribution of the different components of the BA phase of spin-1 BEC on periodic modulation of a_2 scattering channel with amplitude $\alpha = 0.2$ and for frequencies $\omega = \pi/2$ (above) and $\omega = \pi$ (below). The system shows patterns whose wavenumber increases with increasing modulation frequency. Here, the wavenumber of the components corresponding to the unstable density mode is $k = 0.48$ and $k = 0.93$ which compares well with the expected $k = 0.47$ and $k = 0.93$.

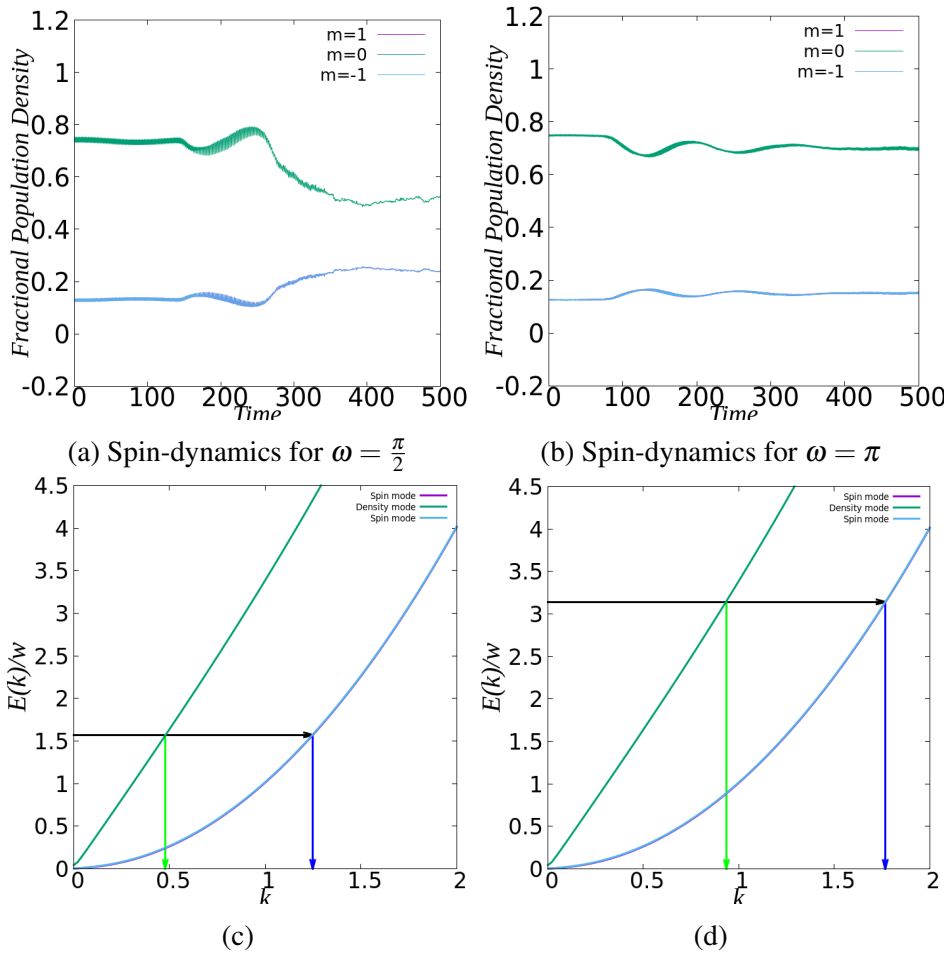

(a) Spin-dynamics for $\omega = \frac{\pi}{2}$ (b) Spin-dynamics for $\omega = \pi$

(c) (d)

Fig. 4.14 Spin-dynamics and dispersion relation of the BA phase with the arrows pointing the most unstable k corresponding to the modulation frequency.

4.2 Summary

- Periodic modulation of the a_2 scattering channel leads to the excitation of spin modes in spin-1 BEC. The exception is ferromagnetic phase for which we see excitation of density mode.
- The excitation of spin modes in the AFM and Polar phase is accompanied with spin dynamics, complex pattern and spin textures formation.
- In the BA phase we observe no spin dynamics and the pattern formation is much simpler with a single wavenumber being excited.
- We do not see patterns indicative of the density mode even though it has parametric instability because the parametric instability associated with the spin mode grows faster.

Chapter 5

Results and Discussions-III

5.1 Periodic modulation of the a_0 and a_2 scattering channels

Periodic modulation of a_0 and a_2 scattering channels simultaneously is given as

$$\tilde{a}_0 = \tilde{a}_0 + \tilde{a}_0(2\alpha_0 \cos(2\omega_0 t)) \tag{5.1}$$

$$\tilde{a}_2 = \tilde{a}_2 + \tilde{a}_2(2\alpha_2 \cos(2\omega_2 t)) \tag{5.2}$$

Modulation of this form requires independent control over the two scattering lengths. This may be achieved by using the method outlined in [30]. We study pattern formation in the different ground state phases of homogenous spin-1 BEC system when a_0 and a_2 scattering lengths modulated simultaneously.We consider two specific conditions to this end:

- a_0 and a_2 scattering lengths modulated at same frequency and amplitude i.e,

$$\alpha_0 \approx \alpha_2 \tag{5.3}$$

$$\omega_0 = \omega_2 \tag{5.4}$$

- a_0 and a_2 scattering lengths modulated at different frequency and amplitude i.e,

$$\alpha_0 > \alpha_2 \tag{5.5}$$

$$\omega_0 > \omega_2 \tag{5.6}$$

We arrive at the equations describing the dynamics of the system on modulation of the scattering lengths by performing a linear stability analysis to test if the translational symmetry may be broken on perturbation of the the uniform system.

5.1.1 Spin-1 BEC in Ferromagnetic Phase

The pattern formation in this phase is unaffected by the modulation of a_0 scattering channel. The reason for this, as mentioned before, is that all two body interactions in this phase are are in the a_2 scattering channel. Hence, the results are exactly same as when the a_2 scattering channel is modulated. We find that Spin-1 BEC in ferromagnetic phase acts almost like a scalar condensate except with spins that are frozen in a single spin state.

5.1.2 Spin-1 BEC in Antiferromagnetic Phase

Homogeneous spinor field for the antiferromagnetic phase in the absence of any perturbation is given below:

$$\left(\sqrt{\frac{1+\frac{p}{c_1}}{2}}, 0, \sqrt{\frac{1-\frac{p}{c_1}}{2}}\right) e^{-i\mu t} \tag{5.7}$$

Here, $\mu = q + c_0 n$.To simplify our calculations we take $p = 0$. We studied pattern formation for uniform system in this phase for the two cases listed below:

a_0 and a_2 scattering lengths modulated at same frequency and amplitude

The equations for the real amplitude of spatial perturbations on performing linear stability analysis for this phase under this modulation condition is given as:

$$\frac{\partial^2 \zeta_+}{\partial t^2} + [(k^2+2c_0)k^2 + k^2(4\tilde{a}_2)(2\alpha\cos(2\omega t))]\zeta_+ = 0 \tag{5.8}$$

$$\frac{\partial^2 \zeta_-}{\partial t^2} + [(k^2+2c_1)k^2]\zeta_- = 0 \tag{5.9}$$

$$\frac{d^2 u_0}{dt^2} + [(k^2+c_1-q)^2 - c_1^2(1-f_z^2)]u_0(t) = 0 \tag{5.10}$$

We get a Mathieu equation for one of the coupled modes,$\zeta_+ = u_+ + u_-$ and a SHO equation for $m = 0$ zeeman component (spin mode) and the other density mode $\zeta_- = u_+ - u_-$. The coupling between the density mode and periodic modulation is evident as the parametric resonance condition in the mathieu equation gives the dispersion relation $\Omega(k) = \sqrt{k^2(k^2+2c_0)}$ of the density mode. The results of numerical simulations are given in Figure- [5.1]. Transla-

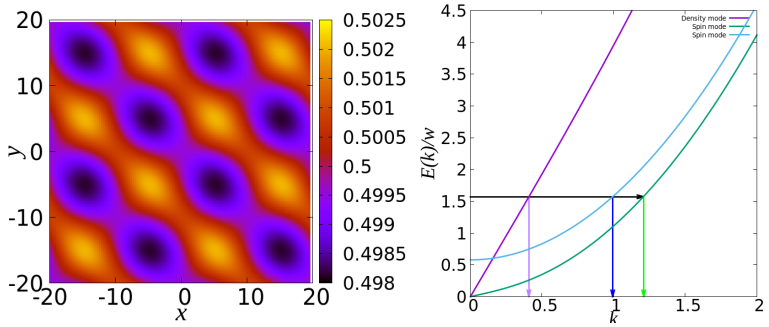

(a) m=1 component (b)

Fig. 5.1 (a)Real space distribution of the spatially modulated components of the AFM phase spin-1 BEC with antiferromagnetic interactions on periodic modulation of both scattering channels with amplitude $\alpha = 0.2$ and for frequency $\omega = \pi/2$. The wavenumber of the unstable mode - density mode is $k = 0.433$ which compares well with the expected $k = 0.42$.(b)Dispersion Relations of AFM phase as a function of wavenumber.

tional symmetry is broken as a result and we see patterns with wave number characteristic of the coupled density mode. The spin modes are stable so there is no population transfer (spin dynamics) or any spin-textures. We can selectively excite the density mode by modulating both scattering channels with same frequency.

a_0 and a_2 scattering lengths modulated at different frequency and amplitude

The equations for the real amplitude of spatial perturbations on performing linear stability analysis for this phase under this modulation condition is given as:

$$\frac{\partial^2\zeta_+}{\partial t^2} + [(k^2+2c_0)k^2 - k^2(2\tilde{a}_0)(2\alpha_0\cos(2\omega_0 t)) - k^2(4\tilde{a}_2)(2\alpha_2\cos(2\omega_2 t))]\zeta_+ = 0 \tag{5.11}$$

$$\frac{\partial^2\zeta_-}{\partial t^2} + [(k^2+2c_1)k^2 - k^2(2\tilde{a}_0)(2\alpha_0\cos(2\omega_0 t)) - k^2(2\tilde{a}_2)(2\alpha_2\cos(2\omega_2 t))]\zeta_- = 0 \tag{5.12}$$

$$\frac{\partial^2 u_0}{\partial t^2} + [(k^2-q+2c_1)(k^2-q) - (k^2-q)(2\tilde{a}_0)(2\alpha_0\cos(2\omega_0 t)) - (k^2-q)(2\tilde{a}_2)(2\alpha_2\cos(2\omega_2 t))]u_0 = 0 \tag{5.13}$$

Here, $\zeta_+ = u_+ + u_-$ and $\zeta_- = u_+ - u_-$. The equations for the real amplitude of spatial modulations is a mathieu equation with two driving frequencies which we cannot solve easily. We look at which mode is most unstable and pattern formation numerically.

Numerical simulations show patterns only corresponding to the a_0 channel being modulated. We do not see any effect of the a_2 scattering channel which was modulated at a lower amplitude and frequency. The patterns in real space and spin-textures show same results as a_0 channel being modulated and a_2 channel is left time-independent.

5.1.3 Spin-1 BEC in Polar Phase

Homogeneous spinor field for the ferromagnetic phase in the absence of any perturbation is given as:

$$(0,1,0)e^{-i\mu t} \tag{5.14}$$

Here, $\mu = c_0$.To simplify our calculations we take $p = 0$. We studied pattern formation for uniform system in this phase for the two cases listed below:

a_0 and a_2 scattering lengths modulated at same frequency and amplitude

The equations for the real amplitude of spatial perturbations on performing linear stability analysis for this phase under this modulation condition is given as:

$$\frac{d^2u_0}{dt^2} + [\Omega^2(\vec{k}) + 4c_0k^2\alpha\cos(2\omega t)]u_0 = 0$$

$$\Omega(k) = \sqrt{k^2(k^2+2c_0)} \tag{5.15}$$

$$\frac{d^2\zeta_+}{dt^2} + [(\Lambda - p)^2]\zeta_+ = 0 \tag{5.16}$$

$$\frac{d^2\zeta_-}{dt^2} + [(\Lambda + p)^2]\zeta_- = 0 \tag{5.17}$$

$$\Lambda = \sqrt{(2c_1 + k^2 + q)(k^2 + q)} \tag{5.18}$$

We get a Mathieu equation for the $m = 0$ zeeman component(density mode) and a SHO equation for the coupled modes,$\zeta_+ = u_+ + u_-$ and $\zeta_- = u_+ - u_-$(spin modes). The coupling between the density mode and periodic modulation is evident as the parametric resonance condition in the mathieu equation gives the dispersion relation $\Omega(k) = \sqrt{k^2(k^2+2c_0)}$ of the density mode. Translational symmetry is broken as a result and we see patterns with wave number characteristic of the $m = 0$ density mode. The spin modes are stable so there is no population transfer (spin dynamics) or any spin-textures. We can selectively excite the density mode by modulating both scattering channels with same frequency. The results of numerical simulations are listed in Figures- [5.2 , 5.3]

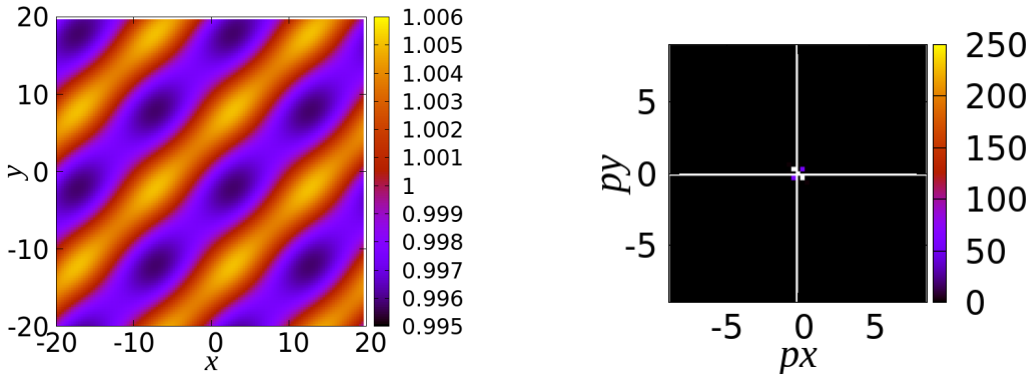

(a) m=0 component (b) m=0 component

Fig. 5.2 Real and momentum space distribution of the spatially modulated components of the Polar phase spin-1 BEC with antiferromagnetic interactions on periodic modulation of both scattering channels with amplitude $\alpha = 0.2$ and for frequency $\omega = \pi$ left. The wavenumber of the unstable mode is $k = 0.468$ which compares well with the expected $k = 0.47$.

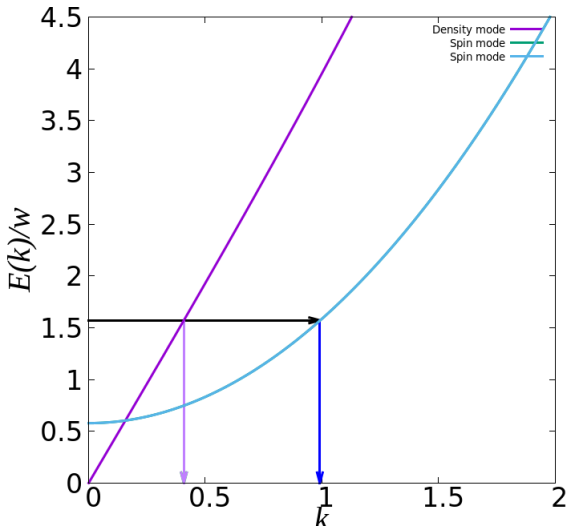

Fig. 5.3 Dispersion Relations of polar phase as a function of wavenumber.

a_0 and a_2 scattering lengths modulated at different frequency and amplitude

The equations for the real amplitude of spatial perturbations on performing linear stability analysis for this phase under this modulation condition is given as:

$$\frac{\partial^2\zeta_+}{\partial t^2} + (k^2+q+c_1)(k^2+q) - (k^2+q)(2\tilde{a}_0)(2\alpha_0\cos(2\omega_0 t))\zeta_+ \qquad (5.19)$$
$$-k^2(4\tilde{a}_2)(2\alpha_2\cos(2\omega_2 t)) = 0$$

$$\frac{\partial^2 u_0}{\partial t^2} + [(k^2+2c_0)k^2 - k^2(2\tilde{a}_0)(2\alpha_0\cos(2\omega_0 t)) \qquad (5.20)$$
$$-(k^2+q)(2\tilde{a}_2)(2\alpha_2\cos(2\omega_2 t))]u_0 = 0$$

Here, $\zeta_+ = u_+ + u_-$. The equations for the real amplitude of spatial modulations is a mathieu equation with two driving frequencies which we cannot solve easily. We look at the most unstable and pattern formation numerically.

Numerical simulations show patterns only corresponding to the a_0 channel being modulated. We do not see any effect of the a_2 scattering channel which was modulated at a lower amplitude and frequency. The patterns in real space and spin-textures show same results as a_0 channel being moodulated and a_2 channel is left time-independent.

5.2 Summary

- We find that the density modes of the spin-1 BEC can be made parametrically resonant by driving both scattering channels at the same time with almost same amplitude and frequency such that only spin-independent interactions are modulated. This kind of modulation suppresses spin-dynamics that might result in creation of parametric instability in the spin-modes.

- Periodically driving the system with different frequencies and amplitudes results in dynamics predominantly due to the channel with the higher amplitude. Dynamics due to periodic modulation of the channel with lower amplitude is suppressed.

Chapter 6

Conclusions and Outlook

The project explored weak excitations in Spin-1 BEC with both ferromagnetic and antiferromagnetic interactions between the spins using periodic modulation of the different s-wave scattering channels for the different ground state phases. It was found that ferromagnetic phase behaves like a scalar condensate which only posses density modes and whose spin modes are never excited under modulation of any scattering channel. Also, like scalar BEC only one scattering channel determines the dynamics of the system i.e, a_2 . It was found that the spin modes of the polar phase, AFM phase and the density mode of the BA phase could be studied by independent modulation of the a_0 and a_2 scattering channels. The density mode of the polar phase and AFM phase can be studied by modulating a_2 and a_0 scattering channels with the same amplitude and frequency. Thus, by modulating the two scattering channels of spin-1 BEC with varied frequencies and amplitudes we can excite and explore different Bogoliubov modes of the spinor BEC.

We were also able to observe spin-dynamics in the system. This was observed when either a_0 or a_2 scattering channel was modulated alone. Spin dynamics occurs as a result of spin-exchange collisions which can transfer population from one component of the spinor BEC to another and back. This has been observed experimentally in Rb-87 spin-1 BEC and Na-23 spin-1 BEC. We also observe spin-textures in the form of domain walls of varied symmetry as a result of spin-dynamics. The spin-textures showed domains that flipped F_x in time.

Exploring pattern formation in traps with varied geometry is currently being pursued. We are especially interested in the variation in spin-textures formed as a result of changing the trap geometry. Spin-currents associated with the spin dynamics and spin-texture also remains to be studied. The system with both scattering lengths modulated with different frequencies remains to be analysed analytically. Periodic modulation results in the heating of the system

and ultimately destruction of the condensate. By including dissipation in the system the time over which patterns are observed can be extended[17].

References

[1] C. C. Bradley, C. A. Sackett, and R. G. Hulet. Bose-einstein condensation of lithium: Observation of limited condensate number. *Phys. Rev. Lett.*, 78:985–989, Feb 1997.

[2] K. B. Davis, M. O. Mewes, M. R. Andrews, N. J. van Druten, D. S. Durfee, D. M. Kurn, and W. Ketterle. Bose-einstein condensation in a gas of sodium atoms. *Phys. Rev. Lett.*, 75:3969–3973, Nov 1995.

[3] Mike H Anderson, Jason R Ensher, Michael R Matthews, Carl E Wieman, and Eric A Cornell. Observation of bose-einstein condensation in a dilute atomic vapor. *science*, 269(5221):198–201, 1995.

[4] D. M. Stamper-Kurn, M. R. Andrews, A. P. Chikkatur, S. Inouye, H.-J. Miesner, J. Stenger, and W. Ketterle. Optical confinement of a bose-einstein condensate. *Phys. Rev. Lett.*, 80:2027–2030, Mar 1998.

[5] Keiji Murata, Hiroki Saito, and Masahito Ueda. Broken-axisymmetry phase of a spin-1 ferromagnetic bose-einstein condensate. *Phys. Rev. A*, 75:013607, Jan 2007.

[6] Michael Cross and Henry Greenside. *Linear instability: basics*, page 56–95. Cambridge University Press, 2009.

[7] Wenxian Zhang, Su Yi, and Li You. Mean field ground state of a spin-1 condensate in a magnetic field. *New Journal of Physics*, 5:77–77, jun 2003.

[8] Hiroki Saito, Yuki Kawaguchi, and Masahito Ueda. Breaking of chiral symmetry and spontaneous rotation in a spinor bose-einstein condensate. *Phys. Rev. Lett.*, 96:065302, Feb 2006.

[9] Leslie Vengalattore Sadler, Higbie and Stamper-Kurn. Spontaneous symmetry breaking in a quenched ferromagnetic spinor bose–einstein condensate. *Nature*, 443, Sept 2006.

[10] Hiroki Saito and Masahito Ueda. Spontaneous magnetization and structure formation in a spin-1 ferromagnetic bose-einstein condensate. *Phys. Rev. A*, 72:023610, Aug 2005.

[11] Dan M. Stamper-Kurn and Masahito Ueda. Spinor bose gases: Symmetries, magnetism, and quantum dynamics. *Rev. Mod. Phys.*, 85:1191–1244, Jul 2013.

[12] S. Lellouch, M. Bukov, E. Demler, and N. Goldman. Parametric instability rates in periodically driven band systems. *Phys. Rev. X*, 7:021015, May 2017.

[13] Tomoki Ozawa, Hannah M. Price, Alberto Amo, Nathan Goldman, Mohammad Hafezi, Ling Lu, Mikael C. Rechtsman, David Schuster, Jonathan Simon, Oded Zilberberg, and Iacopo Carusotto. Topological photonics. *Rev. Mod. Phys.*, 91:015006, Mar 2019.

[14] D. Leibfried, R. Blatt, C. Monroe, and D. Wineland. Quantum dynamics of single trapped ions. *Rev. Mod. Phys.*, 75:281–324, Mar 2003.

[15] Takashi Oka and Hideo Aoki. Photovoltaic hall effect in graphene. *Phys. Rev. B*, 79:081406, Feb 2009.

[16] André Eckardt. Colloquium: Atomic quantum gases in periodically driven optical lattices. *Rev. Mod. Phys.*, 89:011004, Mar 2017.

[17] Kestutis Staliunas, Stefano Longhi, and Germán J. de Valcárcel. Faraday patterns in bose-einstein condensates. *Phys. Rev. Lett.*, 89:210406, Nov 2002.

[18] R. Nath and L. Santos. Faraday patterns in two-dimensional dipolar bose-einstein condensates. *Phys. Rev. A*, 81:033626, Mar 2010.

[19] Jérôme Cayssol, Balázs Dóra, Ferenc Simon, and Roderich Moessner. Floquet topological insulators. *physica status solidi (RRL)–Rapid Research Letters*, 7(1-2):101–108, 2013.

[20] N Goldman, JC Budich, and P Zoller. Topological quantum matter with ultracold gases in optical lattices. *Nature Physics*, 12(7):639, 2016.

[21] M. Krämer, C. Tozzo, and F. Dalfovo. Parametric excitation of a bose-einstein condensate in a one-dimensional optical lattice. *Phys. Rev. A*, 71:061602, Jun 2005.

[22] C. Tozzo, M. Krämer, and F. Dalfovo. Stability diagram and growth rate of parametric resonances in bose-einstein condensates in one-dimensional optical lattices. *Phys. Rev. A*, 72:023613, Aug 2005.

[23] C. E. Creffield. Instability and control of a periodically driven bose-einstein condensate. *Phys. Rev. A*, 79:063612, Jun 2009.

[24] Kazuya Fujimoto and Shun Uchino. Floquet spinor bose gases. *arXiv preprint arXiv:1901.09386*, 2019.

[25] D. J. Papoular, G. V. Shlyapnikov, and J. Dalibard. Microwave-induced fano-feshbach resonances. *Phys. Rev. A*, 81:041603, Apr 2010.

[26] Thomas M Hanna, Eite Tiesinga, and Paul S Julienne. Creation and manipulation of feshbach resonances with radiofrequency radiation. *New Journal of Physics*, 12(8):083031, aug 2010.

[27] Yijue Ding, José P. D'Incao, and Chris H. Greene. Effective control of cold collisions with radio-frequency fields. *Phys. Rev. A*, 95:022709, Feb 2017.

[28] T. V. Tscherbul, T. Calarco, I. Lesanovsky, R. V. Krems, A. Dalgarno, and J. Schmiedmayer. rf-field-induced feshbach resonances. *Phys. Rev. A*, 81:050701, May 2010.

[29] Cheng Chin, Rudolf Grimm, Paul Julienne, and Eite Tiesinga. Feshbach resonances in ultracold gases. *Rev. Mod. Phys.*, 82:1225–1286, Apr 2010.

[30] Peng Zhang, Pascal Naidon, and Masahito Ueda. Independent control of scattering lengths in multicomponent quantum gases. *Phys. Rev. Lett.*, 103:133202, Sep 2009.

[31] L. Zhao, J. Jiang, T. Tang, M. Webb, and Y. Liu. Dynamics in spinor condensates tuned by a microwave dressing field. *Phys. Rev. A*, 89:023608, Feb 2014.

[32] Fabrice Gerbier, Artur Widera, Simon Fölling, Olaf Mandel, and Immanuel Bloch. Resonant control of spin dynamics in ultracold quantum gases by microwave dressing. *Phys. Rev. A*, 73:041602, Apr 2006.

[33] S. R. Leslie, J. Guzman, M. Vengalattore, Jay D. Sau, Marvin L. Cohen, and D. M. Stamper-Kurn. Amplification of fluctuations in a spinor bose-einstein condensate. *Phys. Rev. A*, Apr 2009.

[34] Seji Kang, Sang Won Seo, Joon Hyun Kim, and Y. Shin. Emergence and scaling of spin turbulence in quenched antiferromagnetic spinor bose-einstein condensates. *Phys. Rev. A*, 95:053638, May 2017.

[35] Yuki Kawaguchi and Masahito Ueda. Spinor bose–einstein condensates. *Physics Reports*, 520(5):253–381, 2012.

[36] Michael Cross and Henry Greenside. *Introduction*, page 1–55. Cambridge University Press, 2009.

[37] J. P. Gollub and J. S. Langer. Pattern formation in nonequilibrium physics. *Rev. Mod. Phys.*, 71:S396–S403, Mar 1999.

[38] Michael Cross and Henry Greenside. *Linear instability: basics*, page 56–95. Cambridge University Press, 2009.

[39] P. Engels, C. Atherton, and M. A. Hoefer. Observation of faraday waves in a bose-einstein condensate. *Phys. Rev. Lett.*, 98:095301, Feb 2007.

[40] Alexandru I. Nicolin, R. Carretero-González, and P. G. Kevrekidis. Faraday waves in bose-einstein condensates. *Phys. Rev. A*, 76:063609, Dec 2007.

[41] Kestutis Staliunas, Stefano Longhi, and Germán J. de Valcárcel. Faraday patterns in low-dimensional bose-einstein condensates. *Phys. Rev. A*, 70:011601, Jul 2004.

[42] M. Modugno, C. Tozzo, and F. Dalfovo. Detecting phonons and persistent currents in toroidal bose-einstein condensates by means of pattern formation. *Phys. Rev. A*, 74:061601, Dec 2006.

[43] Alexandru I. Nicolin. Resonant wave formation in bose-einstein condensates. *Phys. Rev. E*, 84:056202, Nov 2011.

[44] Pablo Capuzzi, Mario Gattobigio, and Patrizia Vignolo. Suppression of faraday waves in a bose-einstein condensate in the presence of an optical lattice. *Phys. Rev. A*, 83:013603, Jan 2011.

[45] Kazimierz Łakomy, Rejish Nath, and Luis Santos. Faraday patterns in coupled one-dimensional dipolar condensates. *Phys. Rev. A*, 86:023620, Aug 2012.

[46] Nadav Katz and Oded Agam. Parametrically excited 'scars' in bose–einstein condensates. *New Journal of Physics*, 12(7):073020, jul 2010.

[47] Antun Balaž, Remus Paun, Alexandru I. Nicolin, Sudharsan Balasubramanian, and Radha Ramaswamy. Faraday waves in collisionally inhomogeneous bose-einstein condensates. *Phys. Rev. A*, 89:023609, Feb 2014.

[48] Antun Balaž and Alexandru I. Nicolin. Faraday waves in binary nonmiscible bose-einstein condensates. *Phys. Rev. A*, 85:023613, Feb 2012.

[49] Kazimierz Łakomy, Rejish Nath, and Luis Santos. Faraday patterns in coupled one-dimensional dipolar condensates. *Phys. Rev. A*, 86:023620, Aug 2012.

[50] J B Sudharsan, R Radha, Mihaela Carina Raportaru, Alexandru I Nicolin, and Antun Balaž. Faraday and resonant waves in binary collisionally-inhomogeneous bose–einstein condensates. *Journal of Physics B: Atomic, Molecular and Optical Physics*, 49(16):165303, aug 2016.

[51] Antun Balaž, Remus Paun, Alexandru I. Nicolin, Sudharsan Balasubramanian, and Radha Ramaswamy. Faraday waves in collisionally inhomogeneous bose-einstein condensates. *Phys. Rev. A*, 89:023609, Feb 2014.

[52] LM Symes, RI McLachlan, and PB Blakie. Efficient and accurate methods for solving the time-dependent spin-1 gross-pitaevskii equation. *Physical Review E*, 93(5):053309, 2016.

[53] Wilhelm Magnus and Stanley Winkler. *Hill's equation*. Courier Corporation, 2013.

[54] Y. Castin and R. Dum. Bose-einstein condensates with vortices in rotating traps. *The European Physical Journal D - Atomic, Molecular, Optical and Plasma Physics*, 7(3):399–412, Oct 1999.

[55] A. T. Black, E. Gomez, L. D. Turner, S. Jung, and P. D. Lett. Spinor dynamics in an antiferromagnetic spin-1 condensate. *Phys. Rev. Lett.*, 99:070403, Aug 2007.

[56] L. M. Symes, D. Baillie, and P. B. Blakie. Dynamics of a quenched spin-1 antiferromagnetic condensate in a harmonic trap. *Phys. Rev. A*, 98:063618, Dec 2018.

Appendix A

Spin-1 BEC Quasi-2D system

A.1 Spin-1 BEC System

The Spin-1 BEC system in 3D is described by multi-component Gross-Pitaevskii (GP) equations given below.

$$i\hbar\frac{d\psi_1}{dt} = \frac{-\hbar^2\nabla^2\psi_1}{2M} + V(r)\psi_1 + (-pm+qm^2)\psi_1 \tag{A.1}$$
$$+c_0(|\psi_1|^2+|\psi_0|^2+|\psi_{-1}|^2)\psi_1 + c_1(|\psi_0|^2+|\psi_1|^2-|\psi_{-1}|^2)\psi_1 + c_1\psi_0^2\psi_{-1}^*$$
$$i\hbar\frac{d\psi_0}{dt} = \frac{-\hbar^2\nabla^2\psi_0}{2M} + V(r)\psi_0 + (-pm+qm^2)\psi_0 \tag{A.2}$$
$$+c_0(|\psi_1|^2+|\psi_0|^2+|\psi_{-1}|^2)\psi_0 + c_1(|\psi_1|^2+|\psi_{-1}|^2)\psi_0 + 2c_1\psi_1\psi_{-1}\psi_0^*$$
$$i\hbar\frac{d\psi_{-1}}{dt} = \frac{-\hbar^2\nabla^2\psi_{-1}}{2M} + V(r)\psi_{-1} + (-pm+qm^2)\psi_{-1} \tag{A.3}$$
$$+c_0(|\psi_1|^2+|\psi_0|^2+|\psi_{-1}|^2)\psi_{-1} + c_1(|\psi_0|^2-|\psi_1|^2+|\psi_{-1}|^2)\psi_{-1} + c_1\psi_0^2\psi_1^*$$

We restrict ourselves to two dimensional space, which can be realized by considering a tight pancake shaped potential.In this case the axial confinement energy is so large that the dynamics in the z direction is frozen in the ground state of the strong harmonic potential. Thus, the wave function can be written as [54]:

$$\vec{\Psi}(x,y,z) = \vec{\Psi}(x,y)(\frac{M\omega_z}{\pi\hbar})^{\frac{1}{4}}e^{\frac{-M\omega_z z^2}{2\hbar}} \tag{A.4}$$
$$\vec{\Psi} = \begin{pmatrix}\psi_1\\ \psi_0\\ \psi_{-1}\end{pmatrix}$$

We substitute this in eq[1], eq[2] and eq[3] and integrating out the z- component using eq[5] and eq[6].

$$\int (\frac{M\omega_z}{\pi\hbar})^{\frac{1}{2}} e^{\frac{-M\omega_z z^2}{\hbar}} dz = 1 \tag{A.5}$$

$$\int \frac{M\omega_z}{\pi\hbar} e^{\frac{-2M\omega_z z^2}{\hbar}} dz = \sqrt{\frac{M\omega_z}{2\pi\hbar}} \tag{A.6}$$

We get interaction parameters in 2-dimensions.

$$\tilde{c_0} = c_0\sqrt{\frac{M\omega_z}{2\pi\hbar}} \tag{A.7}$$

$$\tilde{c_1} = c_1\sqrt{\frac{M\omega_z}{2\pi\hbar}} \tag{A.8}$$

The 2-D GPE is given below:

$$i\hbar\frac{d\psi_1}{dt} = \frac{\nabla^2\psi_1}{2M} + V(r)\psi_1 + (-pm + qm^2)\psi \tag{A.9}$$
$$+\tilde{c_0}(|\psi_1|^2 + |\psi_0|^2 + |\psi_{-1}|^2)\psi_1 + \tilde{c_1}(|\psi_0|^2 + |\psi_1|^2 - |\psi_{-1}|^2)\psi_1 + \tilde{c_1}\psi_0^2\psi_{-1}^*$$

$$i\hbar\frac{d\psi_0}{dt} = \frac{-\hbar^2\nabla^2\psi_0}{2M} + V(r)\psi_0 + (-pm + qm^2)\psi_0 \tag{A.10}$$
$$+\tilde{c_0}(|\psi_1|^2 + |\psi_0|^2 + |\psi_{-1}|^2)\psi_0 + \tilde{c_1}(|\psi_1|^2 + |\psi_{-1}|^2)\psi_0 + 2\tilde{c_1}\psi_1\psi_{-1}\psi_0^*$$

$$i\hbar\frac{d\psi_{-1}}{dt} = \frac{-\hbar^2\nabla^2\psi_{-1}}{2M} + V(r)\psi_{-1} + (-pm + qm^2)\psi_{-1} \tag{A.11}$$
$$+\tilde{c_0}(|\psi_1|^2 + |\psi_0|^2 + |\psi_{-1}|^2)\psi_{-1} + \tilde{c_1}(|\psi_0|^2 - |\psi_1|^2 + |\psi_{-1}|^2)\psi_{-1} + \tilde{c_1}\psi_0^2\psi_1^*$$

A.1.1 Making the system Dimensionless

System is scaled with $\hbar\omega_z$, in this case $\omega_z = 2\pi \times 800$. The $n_{peak} = |\psi(\mathbf{x} = 0, t = 0)|^2$(this is used as the homogenous density) value is evaluated for a scalar BEC in a system with $(\omega_x, \omega_y, \omega_z)/2\pi = (10, 10, 800)$ and box size (50,50). This is done for both sodium-23 (Antiferromagnetic Spin-1 BEC) which has $a_0 = 52.746a_b$, $a_s = 50.277a_b$ [55] and Rubidium-87(Ferromnagnetic BEC)$a_0 = 101.8a_b$, $a_s = 100.4a_b$[35]. This evaluation is similar to the procedure outlined in [56]. Lengths in the system are scaled with $\sqrt{\frac{\hbar}{m\omega_z}}$ and listed in table below.

	$\frac{\tilde{c_0} n_{peak}}{\hbar\omega_z}$	$\frac{\tilde{c_1} n_{peak}}{\hbar\omega_z}$	$\frac{\tilde{a_0} n_{peak}}{\hbar\omega_z}$	$\frac{\tilde{a_2} n_{peak}}{\hbar\omega_z}$
Sodium-23	7.32482	0.117971	2.31451	2.48127
Rubidium-87	5.28431	-0.0244482	1.77774	1.75329